Mapping the field around a Langmuir probe with charged dust particles. — Langmuir probe diagnostics are routinely used to determine plasma properties such as electron density and electron energy distribution in gas discharge plasmas [1]. Although this family of experimental techniques is generally considered reliable, the main drawback is that, as an invasive method, the presence of the probe itself alters the properties of the discharge plasmas in its vicinity.
Here we used electrically charged solid dust particles dropped onto a DC voltage biased tungsten probe tip inserted horizontally into an argon capacitively coupled RF discharge (CCP) operated in a GEC Reference Cell to visualize the effect of the probe. Figure 1 shows two cases that differ only in the DC voltage applied to the probe.

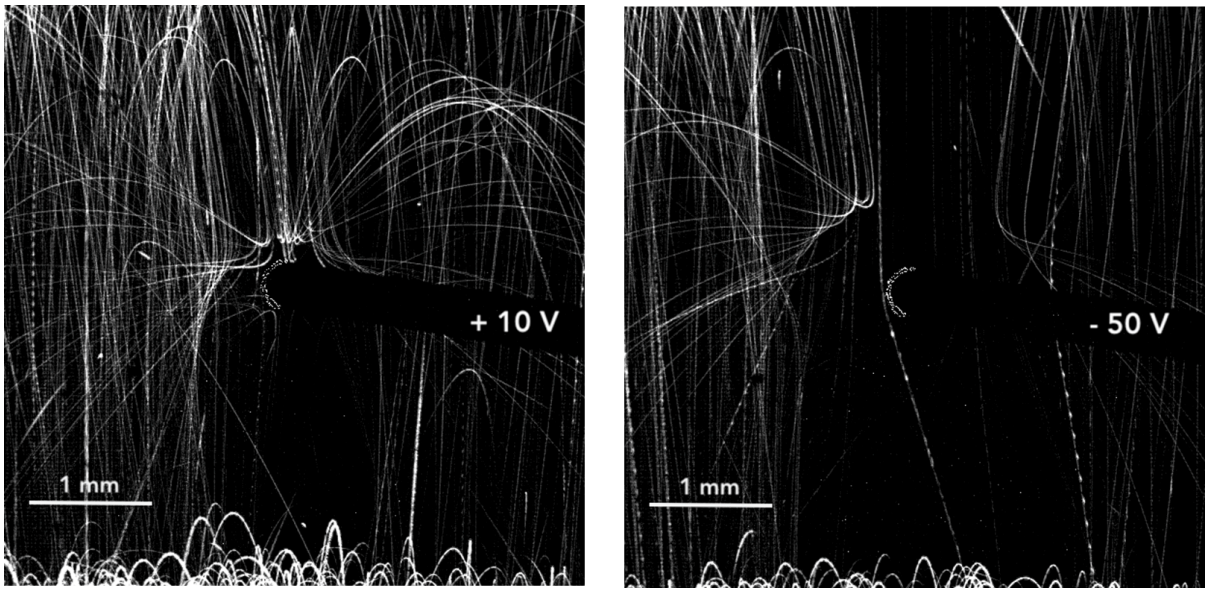

Figure 1: *Dust particles (8.89 mm diameter melamine-formaldehyde) raining down on the probe tip (in the center, 380 mm diameter) illuminated by a vertical laser sheet. The 13.56 MHz CCP discharge is driven in 10 Pa argon gas at approx. 10 W RF power. The DC probe voltages are given in the images.*

When a voltage close to the floating potential (+10 V) is applied to the probe, the particles can get as close as about 0.1 mm before being reflected. In contrast, when a large negative DC voltage (-50 V) is applied, the negatively charged dust particles are strongly repelled at about 1 mm from the probe, but the trajectories of the dust particles closest to the probe tip show deflections characteristic of attractive interaction.
Detailed analysis of the experiments and 2D PIC/MCC gas discharge simulations were performed to gain a deeper insight into the mutual interaction of the probe with the plasma and the dust particles. Figure 2 shows the result of the simulation of the discharge introduced above with -50 V applied to the probe tip. It shows the distribution of the two main force components acting on a charged dust particle in the discharge plasma, namely the electrostatic force and the ion drag force, calculated using the orbital motion limited (OML) theory as derived in [2] using the computed local plasma parameters.

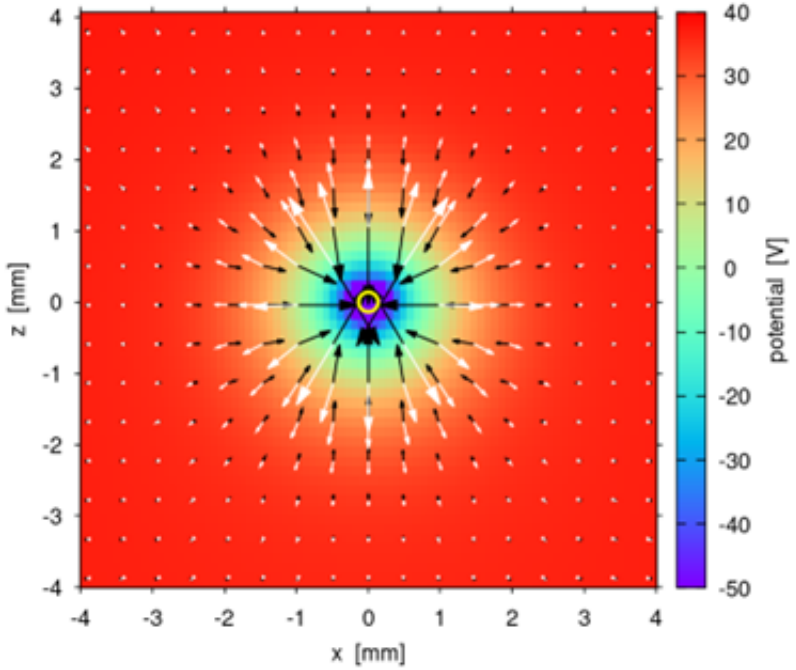

Figure 2: *Electrostatic force (white arrows) and ion drag force (black arrows) acting on negatively charged dust particles (8.89 mm diameter melamine-formaldehyde, -50 V probe voltage). The background color map represents the time averaged electric potential, while the small yellow circle shows the position of the probe wire pointing out of the image.*

Close to the electrode ($r < 0.5$ mm), the ion drag force, caused by the flow of positive Ar^+ ions toward the negatively biased probe, overcomes the electrostatic repulsion between the negatively charged dust particles and the probe, causing a net attraction. At intermediate distances (0.5 mm $< r < 2$ mm) the electrostatic repulsion dominates, while at large distances ($r > 2$mm) both force components disappear.
With this study, we have shown that dust particles are useful tools for resolving the local effect of external perturbations, such as those introduced by Langmuir probes, on gas discharge plasmas. Using dust in plasmas, it is possible to diagnose both the distribution of electrostatic fields and the flow pattern of ions in the discharge.

Comparison of measured and computed optical emission from an argon capacitively coupled plasma – The optical emission spectrum is often used for the experimental characterization of low-temperature plasmas. For a better understanding of the relation between the plasma characteristics and optical emission spectra, first-principle numerical simulations for low-pressure radio-frequency driven capacitively-coupled plasmas (CCPs) in argon gas have been performed by coupling a one-dimensional kinetic particle-in-cell/Monte Carlo collision (PIC/MCC) simulation with a global (zero-dimensional) collisional-radiative model (CRM) [3]. The only ionization and excitation mechanisms included in the PIC/MCC simulations of this study were the electron-impact ionization and excitations of the ground-state Ar atoms, as done commonly in conventional PIC/MCC simulations, whereas the electron-impact ionization of metastable states and other ionization mechanisms were also included in the CRM to account for the optical emission spectra. The PIC/MCC coupled CRM provided the emission spectra of the Ar-I 4p-4s excited level system, which were then compared with experimental optical emission data obtained from the corresponding Ar CCPs, at gas pressures ranging from 2 Pa to 100 Pa. The comparison has shown good agreement for pressures up to about 20 Pa but increasingly notable deviations at higher pressures. The deviation was attributed to the missing consistency between the PIC/MCC simulations and CRM at higher pressures, where the ionization from the metastable states is more dominant than that from the ground states, indicating a significant change in the electron energy distribution function due to the electron collisions with excited Ar atoms at higher pressures. Work is in progress to fully integrate an extended PIC/MCC code and the CRM into a common simulation framework where these modules will be solved iteratively, this way accounting self-consistently for the changes of the electron energy distribution function caused by the stepwise excitation and ionization processes.

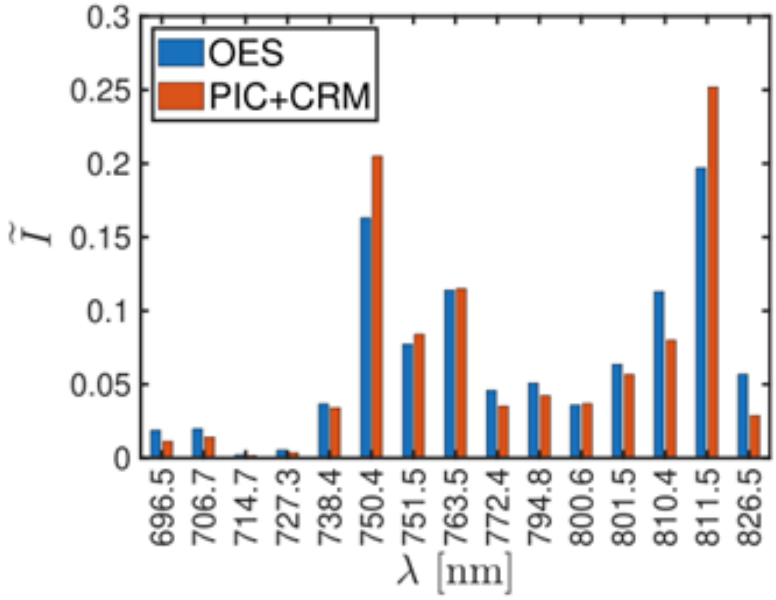

Figure 3. *Measured and computed normalized intensities of prominent Ar-I 4p-4s spectral lines in an argon capacitively coupled plasma at 2 Pa pressure [3].*

Frequency-dependent electron power absorption mode transitions in capacitively coupled argon-oxygen plasmas — Phase Resolved Optical Emission Spectroscopy (PROES) measurements combined with PIC/MCC simulations have been performed to investigate the excitation dynamics in low-pressure capacitively coupled argon-oxygen plasmas. The discharge conditions covered a wide frequency range in a geometrically symmetric plasma reactor operated with a fixed mixture gas composition, at fixed pressure and voltage. The measured and calculated spatio-temporal distributions of the electron impact excitation rates from the Ar ground state to the Ar $2p^1$ state were found to be in good qualitative agreement for all discharge conditions. These results revealed the main differences in the characteristic excitation features at different frequencies (see the time-averaged experimental PROES results in figure 4) and the frequency values around which significant changes in the excitation rate take place. Such changes are generally considered to be predictive of transitions of the dominant electron power absorption mode and discharge operation mode.

Three frequency ranges could be defined with profoundly different characteristic excitation features. : (i) in the low frequency range ($f \leq 3$ MHz), the excitation was found to be strong at the sheaths and weak in the bulk region; (ii) at intermediate frequencies (3.5 MHz $\leq f \leq$ 5 MHz), the excitation rate in the bulk region was found to be enhanced, including the formation of spatially modulated patterns (striations); (iii) above 5 MHz, the excitation in the bulk was found to decrease gradually with increasing frequency. Based on Boltzmann term analysis, the mechanisms behind the excitation characteristics at different frequencies were analyzed. The variation of the number of striations with the frequency was found to have important effects on the contributions of the Ohmic and ambipolar terms to the power absorption. It was found that despite the significantly different excitation maps seen in the different frequency regimes, the dominant power absorption mechanisms are basically the same in frequency ranges I. and II. The results clearly showed that is not straightforward to infer the power absorption mode transitions based on the excitation rate alone as the same electron power absorption mechanisms could be associated with excitation patterns of significantly different characteristics [4].

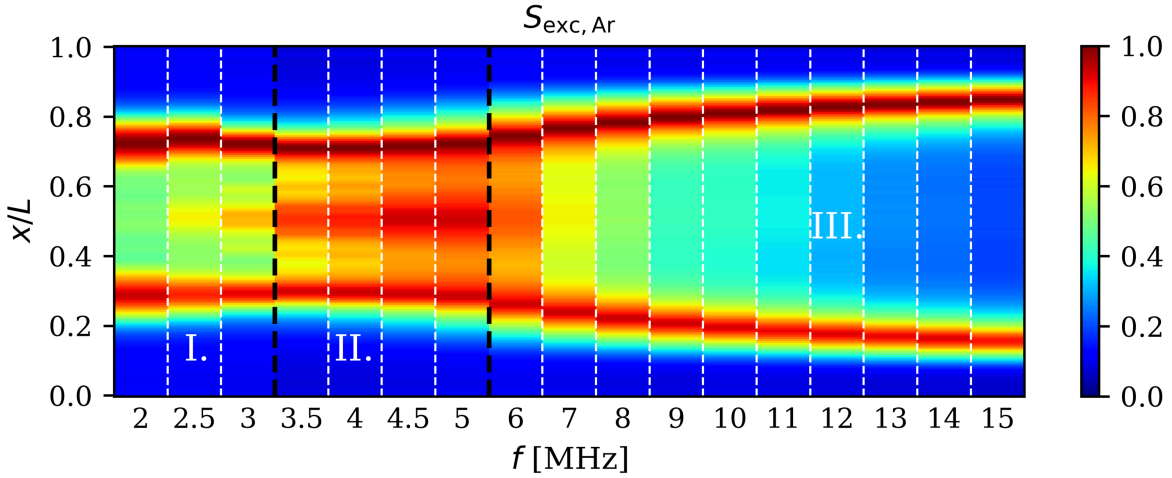

Figure 4: *Time averaged results for the electron impact excitation rate from the ground state into the Ar $2p^1$ state measured by PROES [a.u.] for different driving frequencies (2 MHz ≤ f ≤15 MHz) in 70% Ar - 30% O_2 background gas mixture at a pressure of 120 Pa and peak-to-peak voltage of 350 V. The horizontal axis shows the driving frequency. The vertical axis shows the distance from the powered electrode. The thick vertical dashed black lines indicate the frequency values around which significant changes in the spatial distribution of the excitation rate take place, defining three frequency regimes labeled as I., II. and III. in the figure.*

Plasma-deposited reactive species assisted synthesis of colloidal zinc-oxide nanostructures – Colloidal zinc-oxide nanoparticles have been prepared by ns-laser ablation of a Zn metallic target in RONS-enriched plasma-treated liquids. A new laser ablation set-up has been designed, where the target surface is positioned in the half-focus of the laser focusing lens and at 60-degree angle with respect to the laser axis. This results in oblique laser incidence with large beam width, which leads to asymmetric bubble collapse and thus favours enhanced material ablation. Furthermore, the ablated material leaves the target in a direction different than the laser axis, and a self-developed convective motion of the ablated material insures the decrease of the shielding effect.

The RONS have been deposited into DIW by using an argon surface-wave microwave discharge operating at 25 W input power. The composition of the plasma- treated liquids has been set by the treatment distance i.e. the discharge tube - liquid surface distance. The pH of the plasma-treated liquids has been adjusted by applying reductive, Zn and Mg, metals. The reductive metals are used in powder form and filtrated from the liquid before the laser ablation process. The different plasma-treated liquids are named as PTW for the plasma-treated DIW, PT(W+Zn) and PT(W+Mg) for the plasma-treated DIW with Zn and Mg powder, respectively. By using plasma-treated liquids with different H_2O_2 to nitrate/nitrite concentration ratio, the work has focused on two main questions (i) the effect of the ablation process and of the ZnO NPs on the stability of the RONS and (ii) the effect of the RONS and of the pH on the properties of the created NPs.

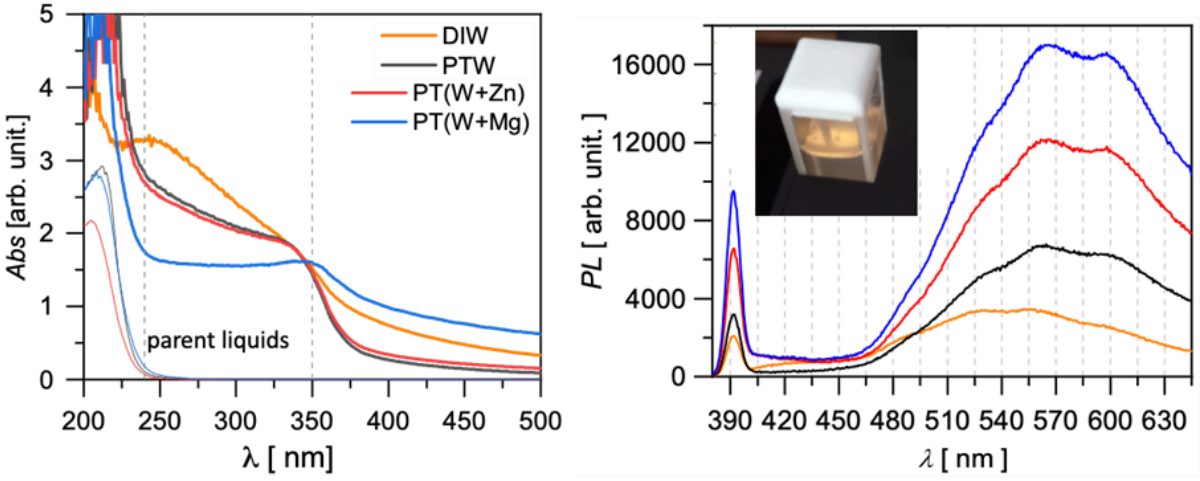

Figure 5: *UV-VIS absorptions spectra and emission using UV excitation in the 275-375 nm spectral range in the case of the DIW-based and plasma-treated liquids based colloids.*

It has been shown that during laser ablation in plasma-treated liquids the H_2O_2 concentration decreases, while in deionized water (DIW) significant H_2O_2 is produced. Meanwhile, the pH increases in the acidic liquids and

decreases in the alkaline ones. During months of storage the pH of colloids stabilize around pH 6, which insures the long-term stability of RONS.

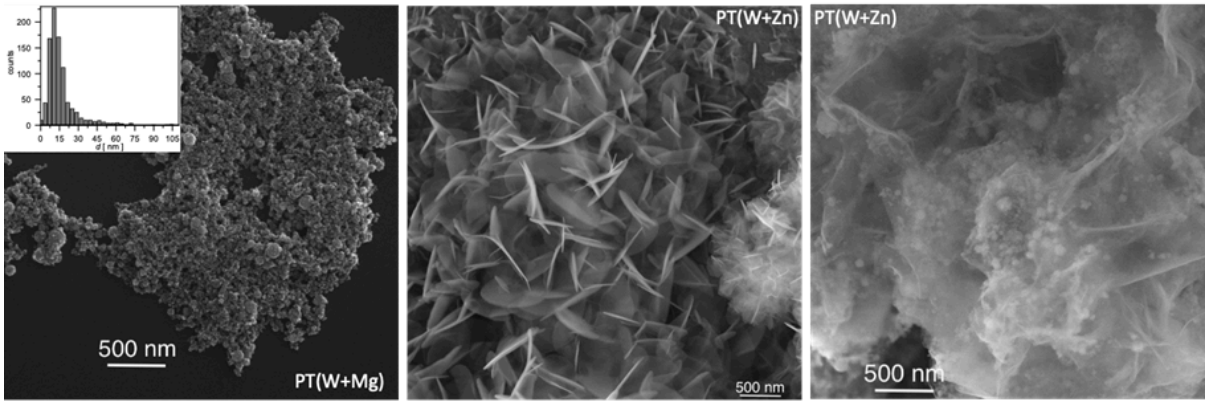

Figure 6: *The SEM images of the ablation product from : (i) a 10 days old PT(W+Mg)- based colloid, (ii) the PT(W+Zn)-based colloid prepared with a 30 s ablation time illustrating the self-assembly of nanosheets, and (iii) a heat treated PT(W+Zn)-based colloid illustrating the nanosheet network.*

It has been demonstrated that in DIW metallic Zn NPs are created, which gradually oxidize during storage, while in the plasma-treated liquids ZnO NPs are produced (see Figure 5) with the mean size of 17 nm (see Figure 6). In the alkaline plasma-treated liquid the NPs form large aggregates, which slows the dissolution of NPs (see Figure 6). In the acidic and neutral solutions besides NPs nanosheets are also formed, which during storage evolve into nanosheet networks as a result of the dissolution of NPs (see Figure 6). The band gap of the colloidal ZnO is found to decrease with the formation of aggregates and nanosheet networks.

The ZnO NPs ablated in plasma-treated liquids exhibit a high-intensity visible emission covering the green-to-red spectral region (see Figure 5). The photoluminescence spectra is dominated by the orange-red emission - previously not detected in the case of laser-ablated ZnO NPs and attributed to the interstitial Zn and oxygen sites - and the yellow emission, which can be attributed to the OH groups on the surface. It has been shown that during months of storage, due to the dissolution of NPs and formation of nanosheets, the intensity of the visible emission decreases and shifts to the blue-green spectral region.

References:

[1] DOI: 10.1088/0963-0252/11/4/320
[2] DOI: 10.1103/PhysRevLett.100.155002
[3] DOI: 10.1088/1361-6595/ad0ede
[4] DOI: 10.48550/arXiv.2307.10319

2022

Radio frequency discharges with structured electrodes - A radio frequency discharge equipped with a structured electrode, operated in helium gas at a frequency of $f = 13.56$ MHz has been investigated experimentally and via kinetic simulations in the $p = 40$ Pa...140 Pa pressure range. 1 cm × 1 cm trenches have been machined into one of the electrodes of the experimental system. In the simulations, only one of these trenches is included with periodic boundary conditions (see figure 1).

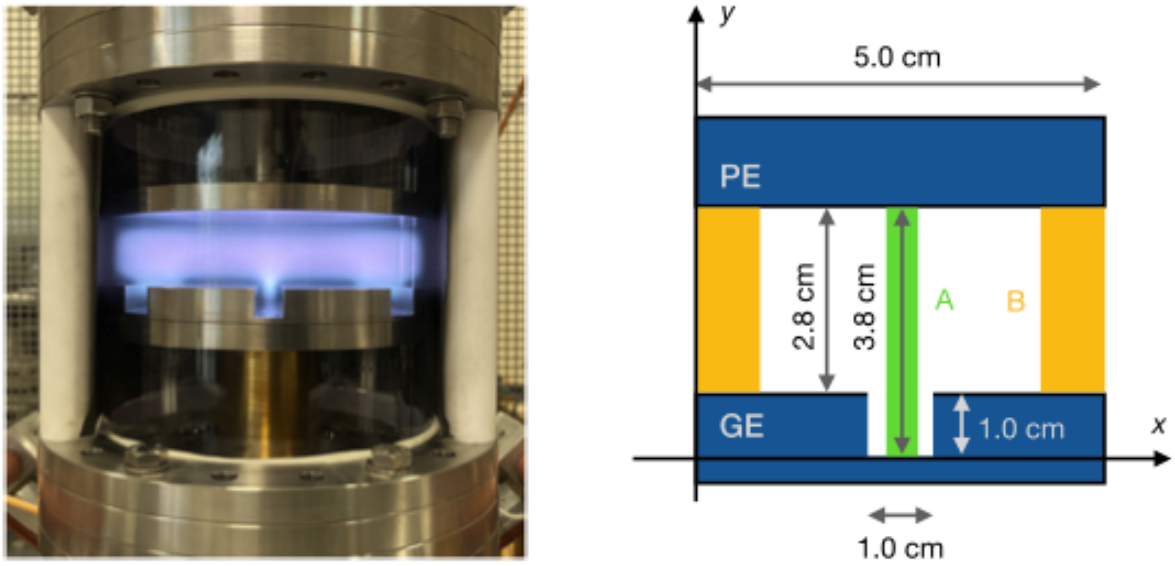

Figure 1. The plasma source with structured electrode in operation in He gas at 60 Pa pressure and 340 V peak-to-peak radio frequency (13.56 MHz) voltage (left) and the dimensions of the electrode configuration (right); based on [1].

This study has been motivated by the understanding the charged particle dynamics and fluxes incident on surfaces in a well-defined two-dimensional model system. In application-relevant scenarios, such as the sterilization or deposition of coatings on medical implants, more complex gas mixtures and surface structures may be present. While these complexities will lead to quantitatively different results, some general application-relevant conclusions can be drawn from the results of this work.

The main experimental diagnostic has been Phase Resolved Optical Emission Spectroscopy (PROES), while the simulations have been based on the particle in cell/Monte Carlo collisions (PIC/MCC) approach, implemented in a novel GPU-accelerated code in 2D Cartesian space. The PROES measurements have been conducted on the He-I 706 nm line and have revealed the 2D temporal dynamics of the excitation rate that is closely connected to the dynamics of the high-energy electrons in the discharge. The excitation rates computed from the PIC/MCC code are found to be in a very good agreement with the experimental data, as shown in figure 2. With an increasing pressure, an enhanced excitation is found within the trench and near its orifice, due to the constructive effect of the sheath expansion at the sidewalls and the bottom part of the trench. Even at low pressures, where no strong excitation within the trench is seen, the most intensive excitation occurred at/near the orifice of the trench.

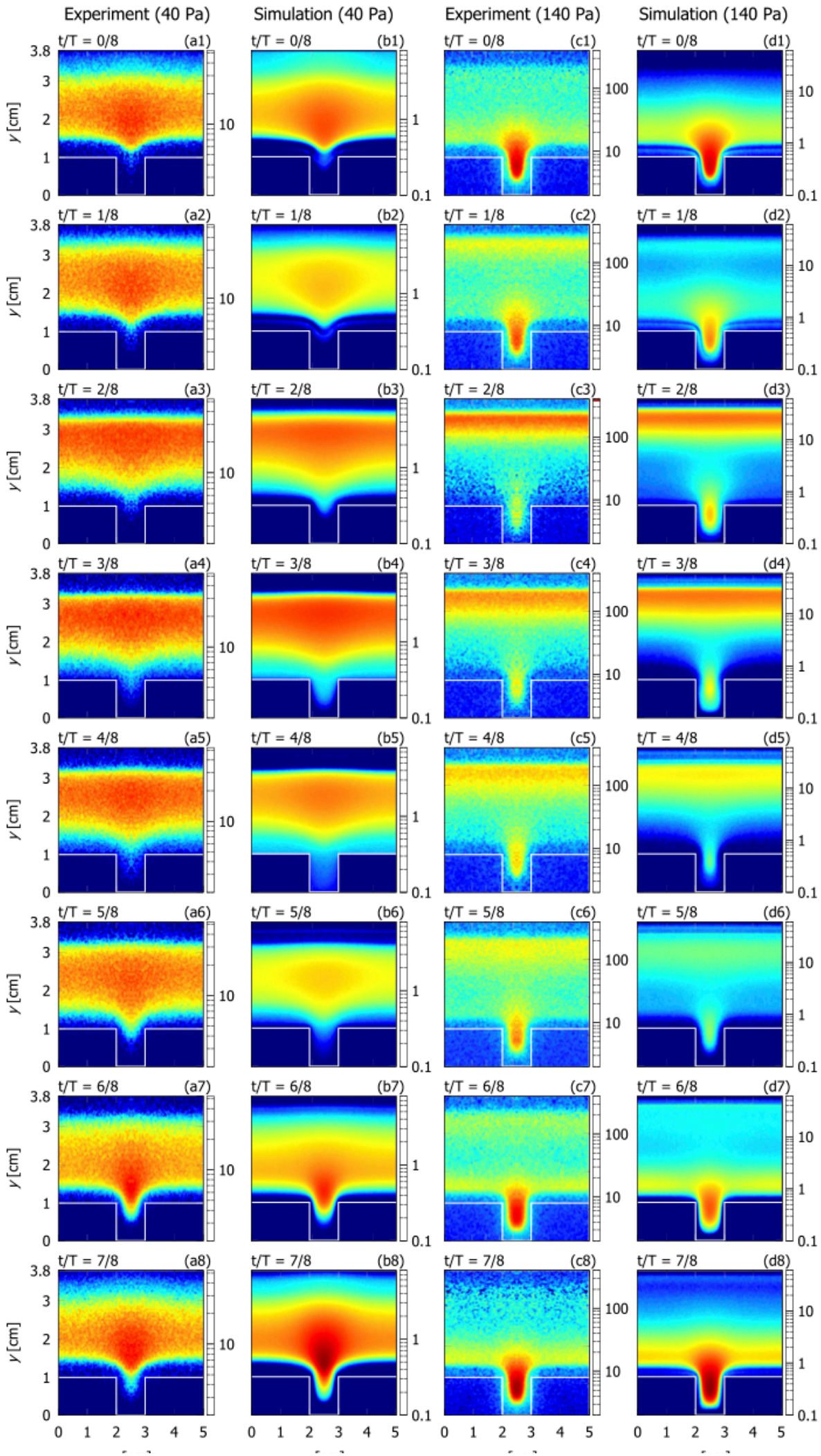
Experiment (40 Pa)
Simulation (40 Pa)
Experiment (140 Pa)
Simulation (140 Pa)
t/T = 0/8 (a1)
t/T = 0/8 (b1)
t/T = 0/8 (c1)
t/T = 0/8 (d1)
t/T = 1/8 (a2)
t/T = 1/8 (b2)
t/T = 1/8 (c2)
t/T = 1/8 (d2)
t/T = 2/8 (a3)
t/T = 2/8 (b3)
t/T = 2/8 (c3)
t/T = 2/8 (d3)
t/T = 3/8 (a4)
t/T = 3/8 (b4)
t/T = 3/8 (c4)
t/T = 3/8 (d4)
t/T = 4/8 (a5)
t/T = 4/8 (b5)
t/T = 4/8 (c5)
t/T = 4/8 (d5)
t/T = 5/8 (a6)
t/T = 5/8 (b6)
t/T = 5/8 (c6)
t/T = 5/8 (d6)
t/T = 6/8 (a7)
t/T = 6/8 (b7)
t/T = 6/8 (c7)
t/T = 6/8 (d7)
t/T = 7/8 (a8)
t/T = 7/8 (b8)
t/T = 7/8 (c8)
t/T = 7/8 (d8)
y [cm]
0
1
2
3
3.8
4
5
10
1
0.1
100

x [cm] x [cm] x [cm] x [cm]

Figure 2. Time evolution of the He 3s 706 nm excitation rate obtained from the experiments (in arbitrary units) and corresponding simulation results (in units of 10^{15} cm^{-3} s^{-1}) for 40 Pa (1st and 2nd columns) and for 140 Pa (3rd and 4th columns). The bottom part of the grounded (structured) electrode (of which the contour is marked by the white lines) is situated at y = 0 cm, while the powered electrode is at y = 3.8 cm. T is the period of the radio frequency excitation. Reproduced from [1].

While excitation and ionization within the trench are found prominent at the highest pressures only, a significant flux of the He^+ ions and VUV resonant photons was found at the surface elements of the trench, for all conditions. Typical values of these fluxes are in the range of 10^{14} cm^{-2} s^{-1}. The mean energy of these ions is found to be couple of 10 eV-s.

Control of ion energy distribution in plasma treatment applications – In a combined experimental and numerical study of capacitively coupled radio frequency, low pressure gas discharges, we have shown that with applying tailored voltage waveforms, composed of low frequency (LF, ~100 kHz) pulsed and high-frequency (HF, >10 MHz) components, it is possible to efficiently decouple plasma generation from the shaping of the ion flux-energy distribution at the electrodes. Details of the experimental setup are shown in the Figure 3. The discharge is operated in 1 Pa argon gas.

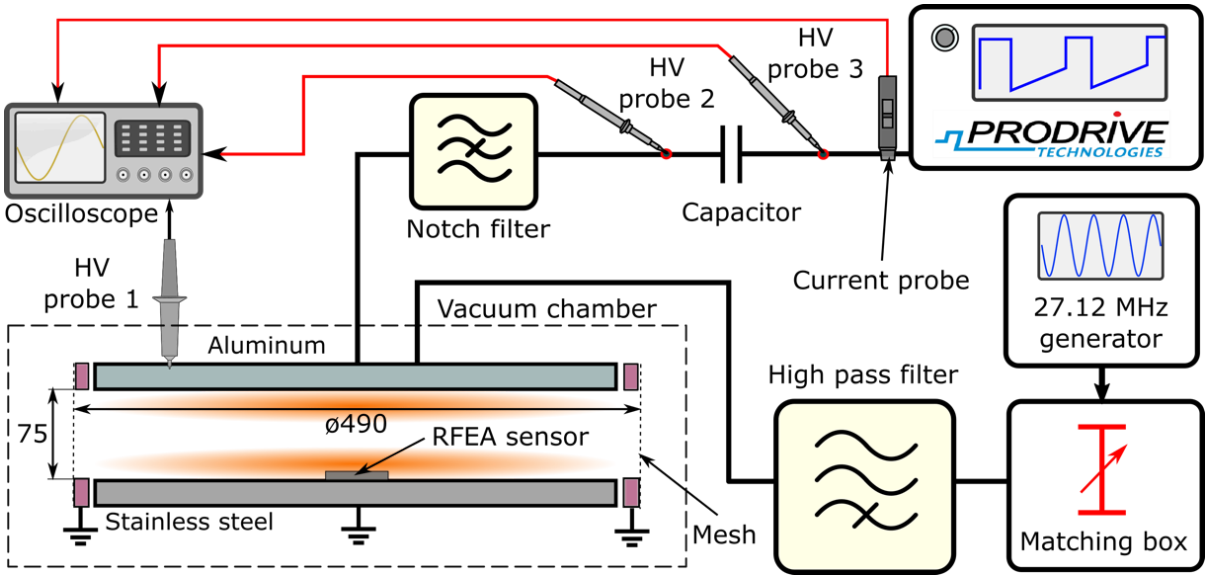

Figure 3. Schematics of the experimental setup with emphasis on the tailored voltage waveform generation circuit. RFEA = retarding field energy analyzer.

In contrast to classical discharges operated at sinusoidal voltage waveforms, a sharp high energy peak can be generated. The amplitude and energy of this peak can be controlled efficiently by tailoring the driving voltage waveform. This is expected to be highly beneficial for a variety of applications such as selective plasma etching. Our findings can be listed as [2]:

• At low duty cycles (D < 30%), during the off-pulse period the discharge operates similarly to a single frequency system. During the positive voltage pulse a strong sheath asymmetry develops, since the LF sheath is fully expanded at the grounded electrode and fully collapsed at the powered electrode. Consequently, the plasma potential rises significantly, and the charged particles are efficiently drained towards the electrodes.
• During the positive pulse, as a consequence of the sheath asymmetry, the sheath expansion electron power absorption mechanism becomes less efficient, resulting in a transient reduction of the plasma density.
• A bi-modal structure of the ion flux-energy distribution forms with peak energies corresponding to the sheath potentials during and after the LF voltage pulse.
• The variation of the LF voltage pulse magnitude couples linearly to the position of the high-energy peak, while is not affecting the low-energy peak of the ion flux-energy distribution at the grounded electrode.
• The peak to background ratio (contrast) of the high-energy peak at the grounded electrode depends on the LF repetition rate, placing a practical upper limit to it for generating a sharp high energy peak.
• The duty cycle of the LF voltage pulse controls the relative magnitudes of the low-, and high-energy peaks of the ion flux-energy distributions. Two regimes, characterized by D < 40% and D > 60% are separated by a transition region. Within each, low and high duty cycle regime, individually, the positions of the spectral peaks are mostly unaffected by the duty cycle.
• The DC self-bias voltage has a direct influence on the peak energies in the ion flux-energy distributions. It is a

parameter sensitive to any kind of asymmetries in the system. Its complex dependence on the duty cycle was used to validate different numerical approaches.

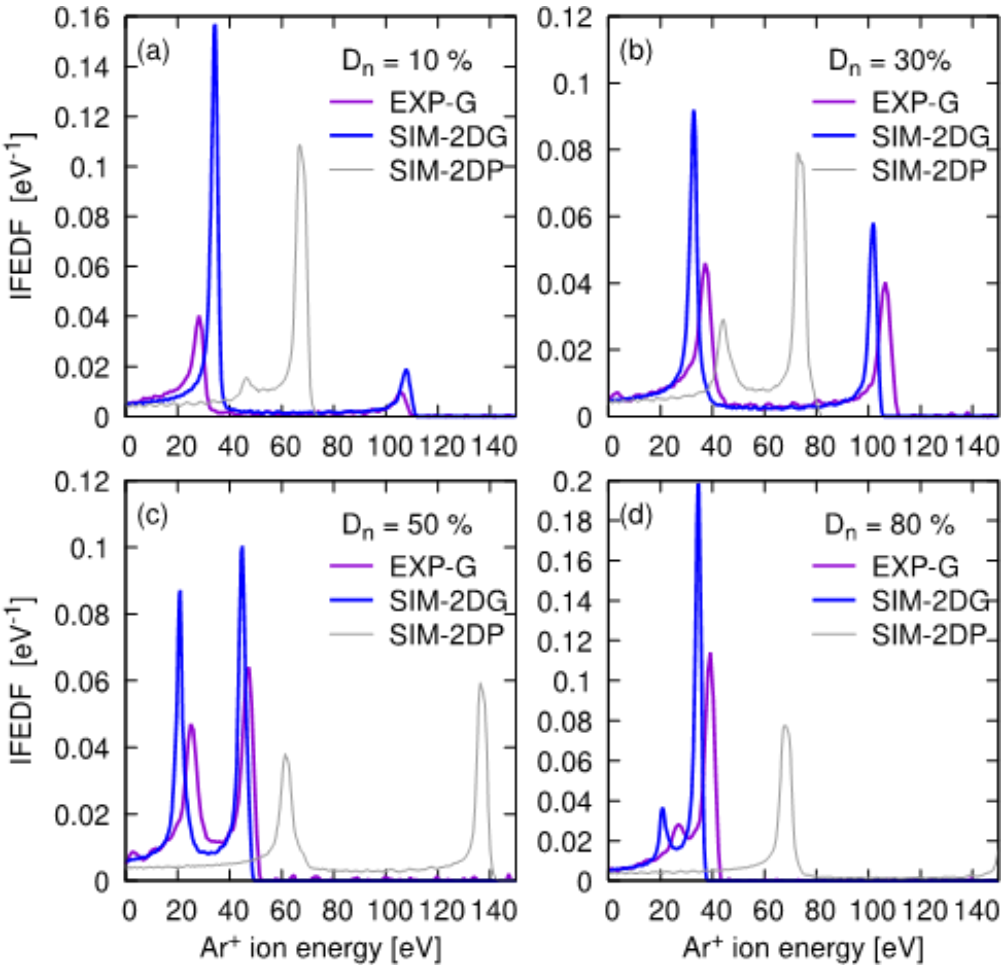

Figure 4. Experimental (EXP) and computed (SIM-2D: axisymmetric two-dimensional particle-in-cell with Monte Carlo collisions modeling) Ar^+ ion flux-energy distribution functions at the grounded (G) and powered (P) electrodes as functions of the LF pulse duty cycle.

The role of metals in the deposition of long-lived reactive oxygen and nitrogen species into the plasma-activated liquids – The application of plasma-activated liquids (PALs) rely mostly on the long-lived reactive oxygen and nitrogen species (RONS), such as H_2O_2, NO_2^- and NO_3^-, which are deposited into the liquids through the plasma-liquid interaction. We have previously shown that the surface-wave microwave discharge is a very flexible system that allows the tuning of RONS concentrations in a wide range. Using this system we are looking for methods that make possible to enhance the deposition of RONS and to ensure their stability during storage of liquids.

During plasma treatment the liquids become acidic, with pH ranging between 3 to 5, which controls the reactions between the RONS during storage, as well as already during the deposition phase. The most important reaction that takes place in the system under acidic conditions is the $NO_2^- + H_2O_2 + H^+ \rightarrow$ products process, which can result in the disappearance of NO_2^- and H_2O_2, respectively, depending on the relative concentrations. In order to control the pH of the plasma treated liquids, we have proposed the use of the high reduction potential metals, such as Mg and Zn, that can reduce H^+ ions into H atoms, which escape from the liquid phase leading to the increase of the pH. The metals are added to the liquids to be treated in powder form, which insures high reaction surfaces, while it is easy to filter out at any stage.

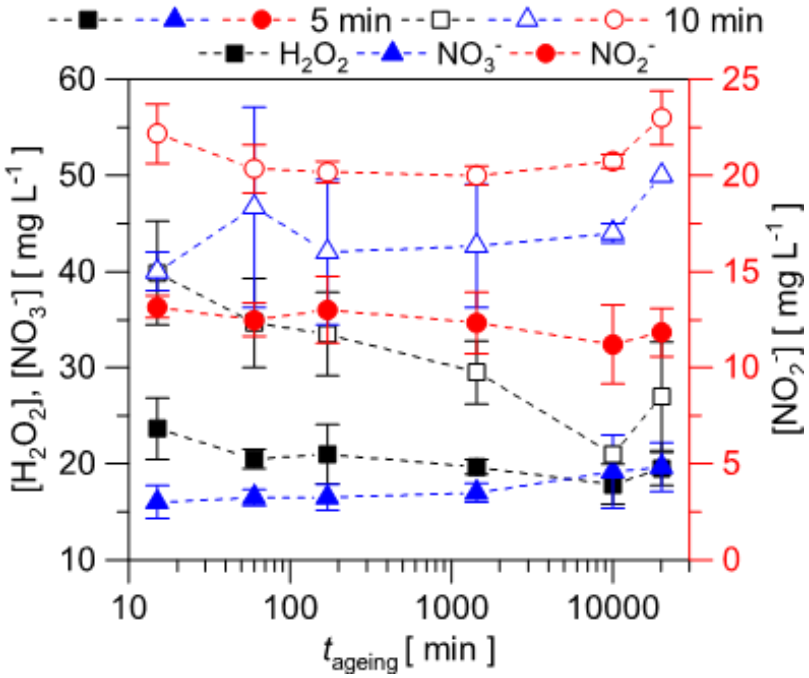

Figure 5. The concentration of reactive oxygen and nitrogen species (RONS) in the filtrated PA(W + Mg) as a function of the storage time in the case of 5 min (closed symbol) and 10 min (open symbol) treatments. The treatment distance is 12 mm. [3]

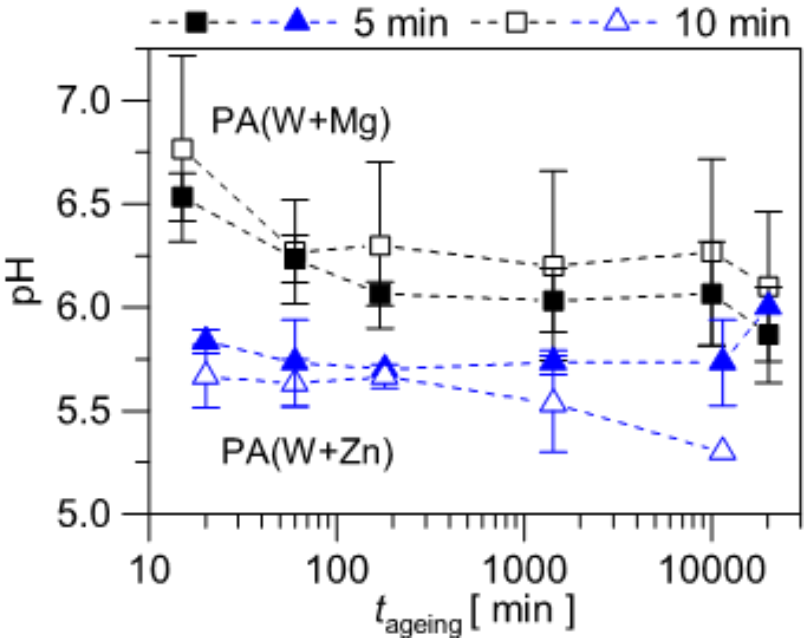

Figure 6. The pH in the filtrated PA(W+Mg) (▫) and PA (W + Zn), respectively, as a function of the storage time in the case of 5 min (closed symbol) and 10 min (open symbol) treatments. The treatment distance is 12 mm. [3]

We have shown, that the composition of the Mg and Zn content plasma-activated waters (PA(W+Mg) and PA(W+Zn)) can be tuned with the system and plasma parameters, while the high reduction potential metals quasi-neutralize the acidification induced by the plasma treatment. As a consequence, in the PA(W+Mg) and PA(W+Zn) significantly higher NO_2^- and H_2O_2 concentrations are obtained than in the PAW, and while in the acidified PAW the NO_2^- production vanishes with increasing of the treatment time, in the PA(W+Mg) and PA(W+Zn) the NO_2^- concentration significantly increases with the treatment time. We have further shown that the filtrated PA(W+Mg) (shown in Figure 5.) and PA(W+Zn) are stable for several weeks. When using the lower reduction potential Zn, at longer treatments (higher RONS deposition) stronger acidification occurs with the pH dropping below 5.5 after the first day of storage (shown in Figure 6.), which results the disappearance of the NO_2^- within the first week. This indicates that the $NO_2^- + H_2O_2 + H^+ \rightarrow$ products process—which is efficient at acidic conditions—in the plasma treated liquids becomes efficient at around pH 5.5. We have reproduced the measured conductivities from the measured species concentrations and showed that a significant contribution comes from the H^+ ions, and thus, the acidified PAW has significantly higher conductivity than the PA(W+Mg) and PA (W+Zn), even with the presence of the dissolved Mg^{2+} and Zn^{2+} ions. We have shown that the concentrations of dissolved metal ions are in the range of those used in the soilless media as plant nutrients. Considering that the pH of the PA(W+Zn) stabilizes below pH 7, we have also studied the plasma-activated ZnNP-colloids, which may have

application relevance. We have shown that the ZnNPs stabilizes the pH of the plasma-activated colloid at around pH 6, which ensures the stability of the RONS concentrations over at least 1 month of storage. Furthermore, the dissolved Zn ion concentrations in PA(W+Zn) and plasma-activated ZnNP-colloid are similar.

Excitation dynamics in low-pressure capacitively coupled plasmas in gas mixtures – PROES measurements combined with PIC/MCC simulations have been performed to study the electron power absorption and excitation/ionization dynamics in low-pressure capacitively coupled neon-oxygen gas mixture plasmas. Such systems, i.e. low-pressure capacitively coupled plasmas in gas mixtures containing oxygen are highly relevant in plasma-based material processing.

This study covers a wide pressure range and a wide mixing range of neon and oxygen gases for a geometrically symmetric plasma reactor with a gap length of 2.5 cm, operated at a driving frequency of 10 MHz and a peak-to-peak voltage of 350 V. The pressure of the gas mixture is varied between 15 Pa and 500 Pa, while the neon/oxygen concentration is changed between 10% and 90%. For all discharge conditions, the spatio-temporal distribution of the electron-impact excitation rate from the Ne ground state into the Ne 3p0 state are recorded by PROES (see figure 7). The experimental PROES results are in good qualitative agreement with the Ne excitation rate obtained from PIC/MCC simulations in the whole parameter regime.

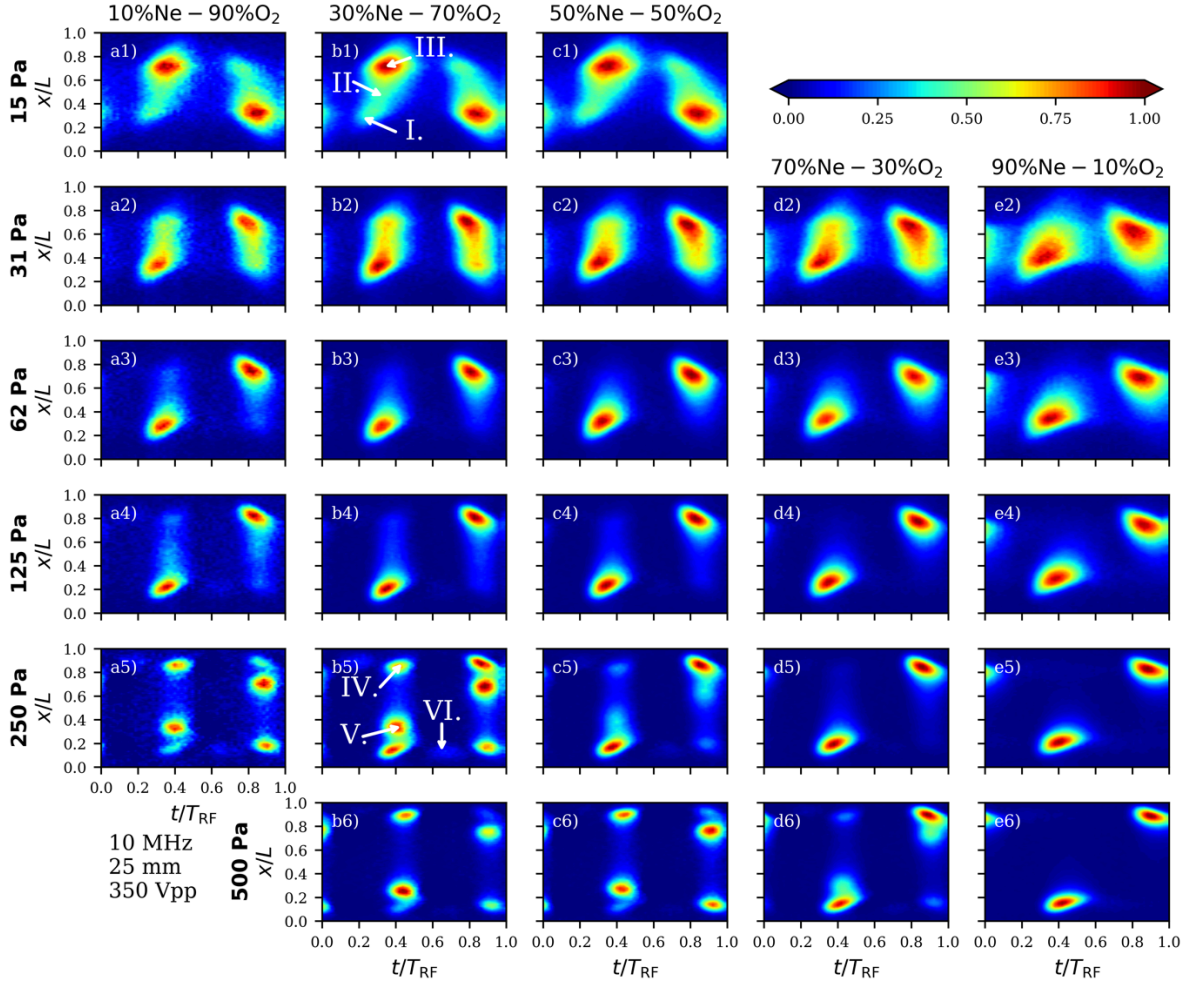

Figure 7. Experimental results. Spatio-temporal plots of the electron impact excitation rate from the ground state into the Ne $3p_0$ state measured by PROES [a.u.] in neon-oxygen capacitively coupled plasmas at different neutral gas pressures: 15 Pa (1st row), 31 Pa (2nd row), 62 Pa (3rd row), 125 Pa (4th row), 250 Pa (5th row) and 500 Pa (6th row), for different neon/oxygen concentration of the background gas mixture (shown in the different columns). The powered electrode is located at x/L = 0, while the grounded electrode is at x/L = 1. The labels I.-VI. in panels (b1) and (b5) indicate the main excitation features found. Reproduced from [4].

Based on the experimental and simulation results, various excitation patterns (labeled as I.-VI. in figure 3) and multiple discharge operation regimes have been identified. At the lowest pressure, weak excitation at the expanding sheath edge (α-peak, I.), weak excitation in the central bulk region (drift feature, II.) and strong excitation at the collapsing sheath edge (ambipolar peak III.) is found in the excitation rates. With increasing pressure, the α-peak and the drift feature are found to be enhanced, while the ambipolar peak is reduced. At intermediate pressures, the α-is found to be the dominant excitation pattern in all mixtures. Further increase of the pressure results in the formation of two distinct excitation peaks at the edges of the bulk region (patterns IV. and V.), which dominates the excitation at high oxygen concentrations. At high pressures and high oxygen

concentrations, weak excitation at the phase of maximum sheath expansion at both electrodes are also observed (γ-peak, VI.).

The mechanisms behind the formation of the various excitation patterns have been revealed based on the PIC/MCC simulation results. It is found that the localized bright emission features at the bulk boundaries at high pressures and high oxygen concentrations are caused by local maxima in the electronegativity. In the wide parameter regime covered in this study, the PROES measurements is found to accurately probe the ionization dynamics in the discharge, i.e. the discharge operation mode.

The simulation shows that the temperature of the electrodes increases significantly compared to the initial wall temperature with increasing the gas pressure. It is found that the power deposition within the gas causes only a slight increase of the gas temperature above the temperature of the electrodes, which is, however, found to be significant due to the heating of the electrodes by the plasma particles.

2021

Kinetic simulation of high-pressure (atmospheric) discharges - Cold Atmospheric Plasmas (CAP) represent a rapidly growing field due to their wide range of applications, e.g., in sterilization, modification of surface properties, as well as in several medical fields, like dentistry, dermatology, and cancer treatment. During the past decades a huge variety of CAP sources have been designed and optimized for these purposes. Among these, Atmospheric Pressure Plasma Jets (APPJ) represent an important class of plasma sources. These devices operate at ambient pressure, usually in a flow of a mixture of an inert gas (He or Ar) and a molecular gas or molecular gases (N_2, O_2, H_2O). Due to the relatively low power consumption the heating of the gas is normally insignificant making these sources applicable for the treatment of temperature-sensitive substances, including biological tissues.

The applications of APPJs are mainly based on the efficient production of reactive oxygen and nitrogen species (RONS) in the gas mixture plasma, therefore optimization of the conditions at which optimum production of RONS can be achieved, is of primary importance. Such studies require both experimental investigations that reveal the charged particle and excitation/ionization dynamics and provide information about the densities of excited species and radicals, as well as modeling of the discharge plasma. In the past years a series of combined experimental and particle simulation studies have been carried out in a collaboration with the Department of Electrical Engineering and Information Science, Ruhr-University Bochum, Germany, to characterize the physics and chemistry of the COST Reference Jet that is a standardized type APPJ source (see, e.g., [1, 2, 3]). These computational studies have used a simplified plasma chemistry model as compared to detailed chemical kinetics modeling investigations but contributed significantly to the understanding of different electron heating modes, mode transitions and the generation of radicals under single- and multifrequency excitation of the discharges.

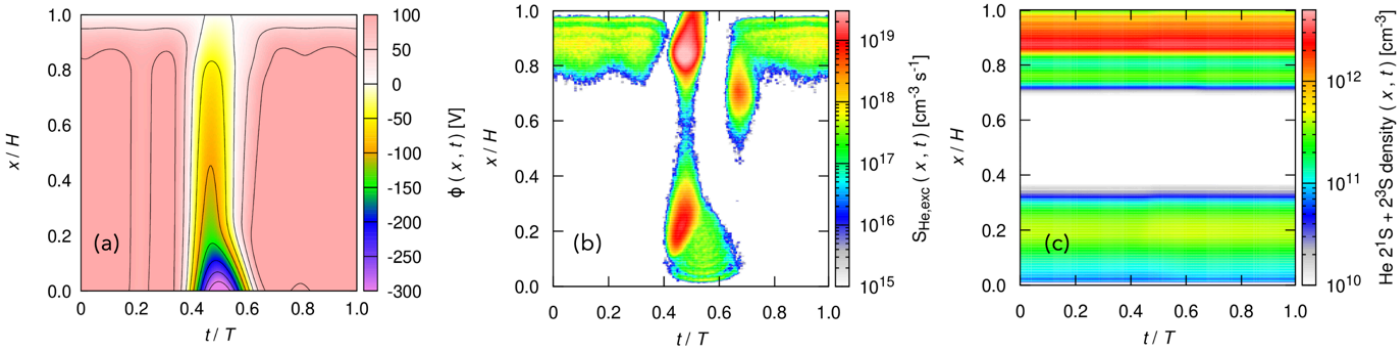

Figure 1. Spatio-temporal distributions of (a) the potential, (b) the total excitation rate of He atoms, and (c) the density of the metastable He atoms. The powered electrode is situated at the bottom (x/H=0) and the grounded electrode is situated at the top (x/H=1). The distance of the electrodes is H = 1 mm, T is the period of the fundamental RF component of the driving voltage waveform.

Figure 1 illustrates the results of a Particle-in-Cell / Monte Carlo Collisions simulation of the plasma source operated in He + 0.1% N_2 gas mixture at 1 bar pressure. The cross section of the source is 1 mm x 1 mm, and its length of the plasma channel is 30 mm. The simulation is 1D and resolves space along the axis that connects the electrodes. The plasma is established by a Tailored Voltage Waveform (TVW) that consists of four harmonics of a base 13.56 MHz radio-frequency (RF) signal and has a peak-to-peak voltage of 475 V, at a “valley” waveform. Panel (a) shows the computed potential distribution between the electrodes, resolved in the inter-electrode space and within the time of one period (T) of the base RF driving voltage. A rapid sheath formation and decay is

observed at the powered electrode around t/T = 0.5, while the sheath at the grounded electrode is expanded most of the time. The specific charged particle dynamics induced by this potential distribution results in a high rate of electron-impact excitation processes, as seen in panel (b) at the sheath expansion of the powered electrode and at the sheath collapse at the grounded electrode (nearly at the same time). The first of the excitation peaks results from the acceleration of the electrons near the edge of the expanding sheath, while the second is a result of an electric field that establishes to drive electrons to the grounded electrode during the short sheath collapse. A significant amount of the excitation events results in the formation of He metastable atoms, which are important excited species. Due to the high density of the background gas the diffusion of these atoms is very slow and their lifetime is comparable to the period of the excitation. He metastable atoms can be destroyed in collisions with N_2 molecules, in Penning-ionization processes. This ionization channel is an important process in the maintenance of the plasma. The density distribution of the He metastable atoms was also measured experimentally and a good agreement with the simulation results has verified the computational model and its implementation.

Electron power absorption in high-pressure (atmospheric) discharges based on the Boltzmann term analysis - Electron power absorption, i.e. the mechanism, by which electrons gain/lose energy in a plasma is a fundamentally important process, whose detailed understanding is of utmost importance for a knowledge based optimization of various plasma processes. A complete, self-consistent description of the electron power absorption dynamics can be gained in low temperature plasmas by the Boltzmann term analysis, a method based on the momentum balance equation, i.e. the first velocity moment equation of the Boltzmann equation, assisted by Particle-In-Cell/Monte-Carlo-Collisions simulations.

This method has been applied to investigate electron power absorption in atmospheric pressure microplasma jets driven by tailored voltage waveforms (TVW) operating in a gas mixture of helium and nitrogen. Using tailored voltage waveforms allows for the possibility to enhance and adjust the generation of selected neutral species by controlling the electron power absorption dynamics, however, the fundamental reason for why this is possible had been unclear. Using the Boltzmann term analysis, an answer can be found to this question [4].

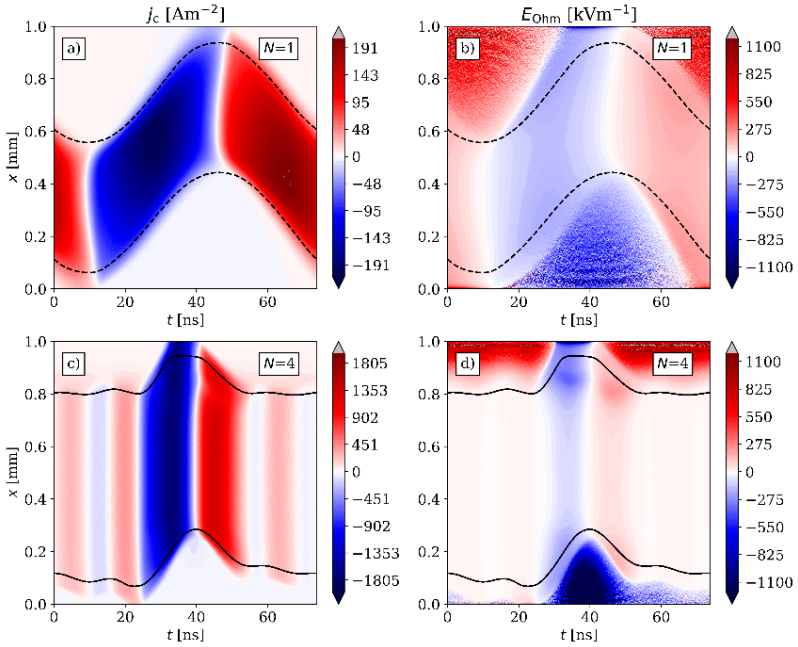

Figure 2. Spatio-temporal distributions of the conduction current density and the ohmic electric field for a single harmonic waveform (a,b) and a valleys type waveform of four harmonics (c,d). The powered electrode is situated at the bottom (x=0) and the grounded electrode is situated at the top (x=1 mm). The (dashed) black lines indicate the sheath edges.

The main reason behind the aforementioned control is fundamentally related to the fast sheath collapse in case of a valley-type waveform as shown in Figure 2 (c,d), which is absent for a single frequency discharge (Figure 2 (a,b)). In Figure 2 (c), near 0.8 mm the sheath abruptly decreases, leading to a high electron current density in this region because of flux conservation. In order for such a high current density to be able to flow through the discharge, a correspondingly high electric field has to be present. As shown in Figure2 (d), this is primarily an Ohmic field, a consequence of the locally decreased electron density, as calculated from the Boltzmann term analysis. Due to the high current density and electric field, in this region a high electron power absorption is present, which can lead to a localization of the generation of certain radicals.

Plasma-activated liquids for agriculture and medicine - In the last decade plasma-activated water (PAW), or more generally plasma-activated liquid (PAL) has received a lot of attention from the plasma medicine and plasma agriculture community due to its potential to induce oxidative stress to cells. As a consequence PAL can have antimicrobial, antibacterial and antitumor properties, while it can also be used for priming to increase the stress tolerance of cells. PAL is created through the interaction of active or afterglow plasma with the liquid, when reactive species, mostly reactive oxygen and nitrogen species (RONS), are generated in the liquid phase, which play the major role in the oxidative processes. The applications rely mostly on the long-lived RONS, such as H_2O_2, NO_2^- and NO_3^-, and use PALs of different RONS composition. In 2019 we have shown that the surface-wave microwave discharge is a very flexible system that allows the tuning of RONS in PAW in a wide concentration range. However, during storage the PAL's composition changes due to the reaction between the RONS. This fact calls for the need of methods that can stabilize the PAL's composition. Recently, we have demonstrated that the ageing of PAL can be controlled by taking advantage of the Fenton-type of reaction using Cu-ions originating from different copper surfaces immerged into the PAL [5]. In this way the PALs can be kept quasi-stable for several weeks.

In the field of medicine the interest lies in the plasma-activated physiological solutions, such as Buffered Phosphate Saline (PBS) or Ringer's solution. Although physiological solutions have been proven to kill selectively cancer cells and allow for local delivery by injection into the tumor, they can be quickly washed away by body fluids. To overcome this the use of plasma- activated gelatin solutions has been suggested. For this purpose, we have proposed a new protocol for trapping RONS in gelatin without the direct plasma treatment of the gelatin solution. This method based on the use of plasma-activated liquids has the advantage to prevent the cross-linking of the gelatin that may occur by plasma treatment, and also to overcome the diffusion limited deposition of RONS due to the gelation of the solution. We demonstrated that the H_2O_2 , NO_2^- and NO_3^- concentrations are quasi-stable during one month of storage in the 0.5% - 2% gelatin solutions prepared with plasma-activated water, plasma-activated Ringer's and PBS solutions, respectively, as also illustrated in Figure 3. The NO_2^- is efficiently trapped even at acidic pH 4.5-5.5 conditions due to the protein network developed with gelation. [6]

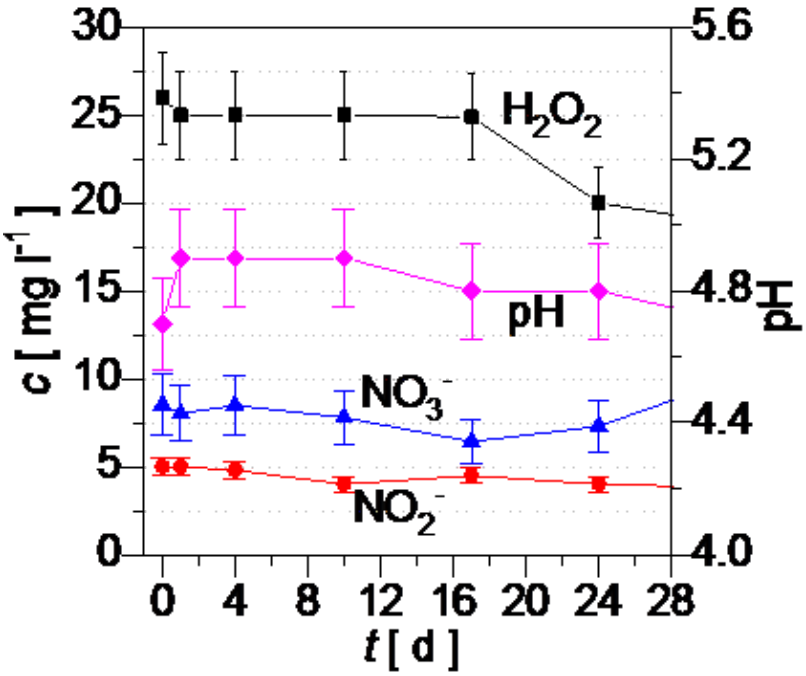

Figure 3. Evolution of the species concentrations and the pH during storage in the 2% gelatin solution prepared with plasma-activated water produced with the surface-wave microwave discharge.

Self-Organized Dust Chains in DC discharges - The self-organization of dust grains in a flowing plasma offers insight into the interplay among charged species in a complex plasma environment, relevant to astrophysical and technological systems. In a complex plasma, micrometer sized particles (also known as "dust") acquire charge due to interactions with ions and electrons. Ground-based experiments have studied the formation of dust structures, in the sheath region of a gas discharge plasma, where a large vertical electric field is required to balance the gravitational force acting on the dust particles. Ions drift relative to the more massive dust grains, with the ion drift velocity corresponding to the strength of the applied electric field. The trajectories of ions in the vicinity of a charged dust grain are deflected, leading to the build-up of ion clouds downstream from the dust grain, forming a region of enhanced ion density called an ion wake. The presence of positively charged ion wakes is thought to be responsible for the non-reciprocal interactions that have been observed between negatively charged dust grains in a flowing plasma.

In contrast, microgravity dusty plasma experiments performed on parabolic flights or on the International Space Station (ISS) enable investigations of dust dynamics in the near-absence of gravitational influence, where the smaller effects from the dust-dust, dust-ion, and drag forces are the primary drivers of the dust motion. In microgravity experiments, the dust cloud can be levitated within the bulk of the discharge plasma where electric fields are weaker, and ion flow speeds are lower, than typically found in a plasma sheath.

The most recent iteration, the Plasmakristall-4 (PK-4) experiment, has implemented a long axial direct-current discharge tube (instead of the compact radiofrequency, RF, plasma used in previous iterations of the Plasmakristall experiments) to further aid investigations of the liquid state of complex plasmas.

In a recent study, in collaboration with the Center for Astrophysics, Space Physics & Engineering Research (CASPER) at Baylor University, Waco, Texas, we have performed multi-scale numerical modeling, assisted by lab-based experiments, of the PK-4 dusty plasma system connecting the electron dynamics at the nanosecond timescale with the neon ion properties at the microsecond timescale, and described the dust particle motion in the millisecond time domain [7]. We could identify the presence and quantify the properties of fast ionization waves in the discharge, and further compute the motion and self-organization of the dust particle in such plasma environment. Our results closely match the observations made during a recent campaign of the PK-4 experiment on board the ISS and provide detailed microscopic data for the verification of phenomenological dust particle charging models [8].

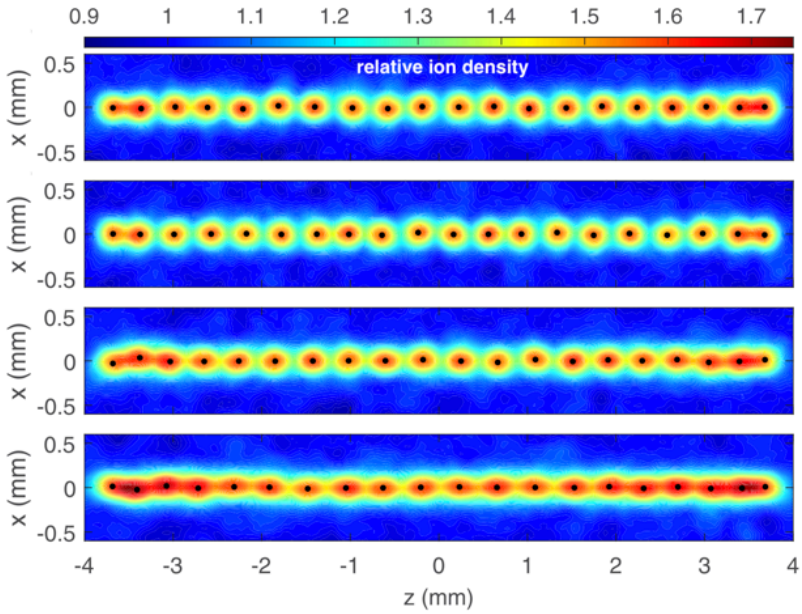

Figure 4: Neon ion density distribution (relative to the background value) around the dust particles for different periods of the oscillating plasma environment during the crossing of ionization waves.

Surface processes in low-pressure Capacitively Coupled Plasmas - Low-pressure Capacitively Coupled Plasmas (CCPs) are essential for modern plasma processing technologies: they are widely used in applications, such as etching of semiconductors, plasma-enhanced chemical vapor deposition, reactive sputter deposition, or surface treatment of medical interest. Such technological plasmas, frequently operated in complicated mixtures of reactive gases, require specific flux-energy distributions for electrons, ions and neutrals. Optimized process control is generally not possible in conventional single-frequency CCPs, while limited control can be achieved for dual-frequency discharges operated at significantly different frequencies. A highly promising way to achieve an advanced control of distribution functions is driving CCPs with tailored voltage waveforms (generated as a superposition of multiple harmonics of a fundamental driving frequency). There are a variety of phenomena that are not well understood in these plasmas. Therefore, the applications are generally optimized by empirical methods rather than based on complete understanding of the physics of such plasmas. In the past years several studies have been performed to clarify the underlying physics in such systems, including the clarification of the influence of the surface material and various surface processes, such as the electron and ion induced secondary electron emission (SEE), surface recombination of excited species and radicals, on the plasma parameters and efficient control of particle properties.

The Particle-in-Cell/Monte Carlo Collisions (PIC/MCC) kinetic simulation method is a widely applied tool for the computational study of CCPs. While many efforts have been taken to model the gas phase processes of CCPs precisely in PIC/MCC simulations, the surface processes are often neglected or considered with rough simplifications in such simulations. A constant elastic reflection coefficient is often applied for the electrons hitting the electrode surface, and constant SEE coefficient is often applied for the ions. In the 2018-2020 period in our studies, realistic surface models have been incorporated to the discharge models. For the electrons, elastic and

inelastic reflection and SEE induced by them have been considered with realistic coefficients that depend on the energy and the angle of incidence of the incoming electron. For the heavy particles (ions, fast atoms/molecules), SEE and sputtering have been considered with energy-dependent coefficients. Measured gas temperature values were also considered in the simulations [9].

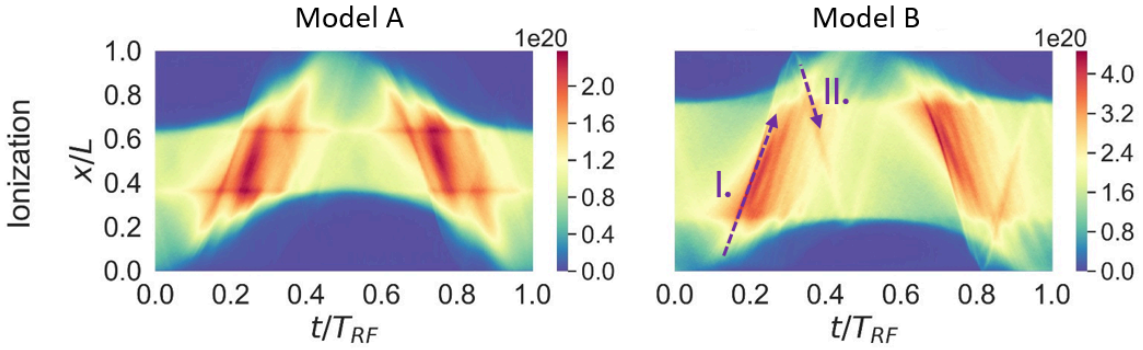

Figure 5. Spatio-temporal distribution of the ionization rate [$m^{-3}s^{-1}$] obtained from PIC/MCC simulations based on a discharge model in which simple approaches are used for the description of the surface processes (model A) and that obtained by describing the surface processes realistically (model B). The dashed lines in the right panel indicate the strong ionizing beams related to secondary electrons. Discharge conditions: O_2 gas, SiO_2 electrodes, L = 6.7 cm, p = 0.7 Pa, V_0 = 1000 V, f = 13.56 MHz. [9]

In Figure 5, the PIC/MCC simulation results for the spatio-temporal distribution of the ionization rate are compared according to two different surface models for oxygen CCPs operated between SiO_2 electrodes, at a low pressure of 0.7 Pa. Model A is a simple model assuming a constant elastic reflection coefficient of $\eta_e = 0.2$ for the electrons and a constant SEE coefficient of $\gamma = 0.4$ for the ions. In model B, a realistic model is used for the electrons considering elastic and inelastic reflection and SEE with energy-dependent coefficients, and $\gamma = 0.4$ is used for the O_2^+ ions. According to model A, the O_2 discharge operates in drift-ambipolar mode, which is typical in electronegative discharges. However, model B, which includes electron-induced SEE, exhibits α-mode (beam I.), and an additional ionizing beam appears at the phase of partial sheath collapse (beam II.). This second beam was found to consist of only secondary electrons originating from the electrodes. Meanwhile, the electronegativity of the discharge was found to significantly decrease due to electron-induced SEE.

2020

Ionization waves in microgravity dusty plasma experiments. — The PK-4 system is a micro-gravity dusty plasma experiment, utilizing a long DC discharge in neon or argon gases, currently in operation on the board of the International Space Station. The local plasma parameters that serve as input data for dust dynamics models were calculated by our recently developed 2D particle-in-cell with Monte Carlo collisions discharge. The simulations further show that on the microsecond time scales the positive column is highly inhomogeneous: ionization waves with phase velocities in the range between 500 m/s and 1200 m/s dominate the structure, where the electric field and charged particle densities can reach amplitudes up to 10 times of their average value. In our ground-based PK-4 replica system the direction of the DC current can be alternated, which favours the dust particle chain formation. [1]

Soliton propagation in a strongly coupled dusty plasma layer. — We have investigated by Molecular Dynamics simulations the propagation of solitons in a two-dimensional many-body system with Yukawa potential. The solitons were created in an equilibrated system by short electric field pulses. These pulses were found to generate pairs of solitons, with a positive and a negative density peak, respectively, which propagated into opposite directions. At small perturbations, these features were confirmed to propagate with the longitudinal sound speed, from which an increasing deviation was found at higher amplitude perturbations. The application of an external magnetic field was found to block the propagation of the solitons, which were, however, found to get released upon the termination of the magnetic field and could propagate further into directions that depend on the time of trapping and the magnetic field strength. [2]

Control of heavy particle's energy and flux in low-pressure capacitively coupled radio frequency (rf) discharges. — Particle-in-Cell/Monte Carlo Collisions simulations of capacitively coupled Ar discharges driven by multi-frequency tailored voltage waveforms were performed, in order to clarify the effects of surface processes on the discharge characteristics. The simulations were based on a discharge model in which realistic approaches were implemented for the description of the secondary electron emission induced by electrons and heavy-particles at the electrodes, as well as for the sputtering of the electrodes. The simulations showed that the mean energy of Ar+ ions and fast Ar atoms, as well as the flux of sputtered atoms can be controlled at both electrodes by changing the phases of the even harmonics. The domain over which the sputtered atom flux can be varied was found to be enlarged by adding more harmonics to the driving voltage waveform. [3]

Electron power absorption in low-pressure capacitively coupled rf argon discharges — We conducted a spatio-temporally resolved analysis of the electron power absorption in capacitively coupled argon plasmas (CCPs) at low pressures (1–10 Pa), based on the 1D momentum balance equation embedded into 1d3v particle-in-cell/Monte Carlo collisions simulations. In contrast to the predictions of theoretical models, the 'Ohmic heating' is found to be the dominant electron power absorption mechanism on time average at the lowest pressures, and not the 'stochastic' or 'Pressure heating', as one would expect. This is attributed to the attenuation of the electron power absorption due to the electron acceleration by the 'ambipolar' electric field on time average at low pressure, which is a consequence of the collisionless transit of energetic beam electrons generated during sheath expansion at one electrode to the opposite electrode. These energetic electrons arrive during the local sheath collapse and thus can be lost on the surface. As a consequence, the plasma density decreases and the electron temperature becomes temporally more symmetric within the RF period compared to that in discharges operated at higher pressures, which causes a reduction of 'Pressure heating' on time average. [4]

Electron power absorption mode transitions in neon capacitively coupled rf discharges — The spatio-temporal ionization and excitation dynamics in low-pressure radiofrequency (RF) discharges operated in neon were studied by phase resolved optical emission spectroscopy (PROES) and by particle-in-cell/Monte Carlo collisions (PIC/MCC) simulations. At a fixed frequency and peak-to-peak voltage, the spatio-temporal distribution of the ionization rate obtained from PIC/MCC showed a transition of the discharge operation mode from the α-mode to the γ-mode with pressure. In the spatio-temporal distribution of the excitation rate obtained from the PROES and PIC/MCC the *α*-peak (the intensity maximum at the bulk side of the expanding sheath edge) was dominant, while a γ-peak (a maximum near the edge of the fully expanded sheath) became visible only at higher values of the pressure (500 Pa) or at the lowest frequency of 3.39 MHz. On the other hand, a γ-peak was visible in the ionization rate for all operation conditions, and it dominated the ionization in the vast majority of the cases investigated. [5]

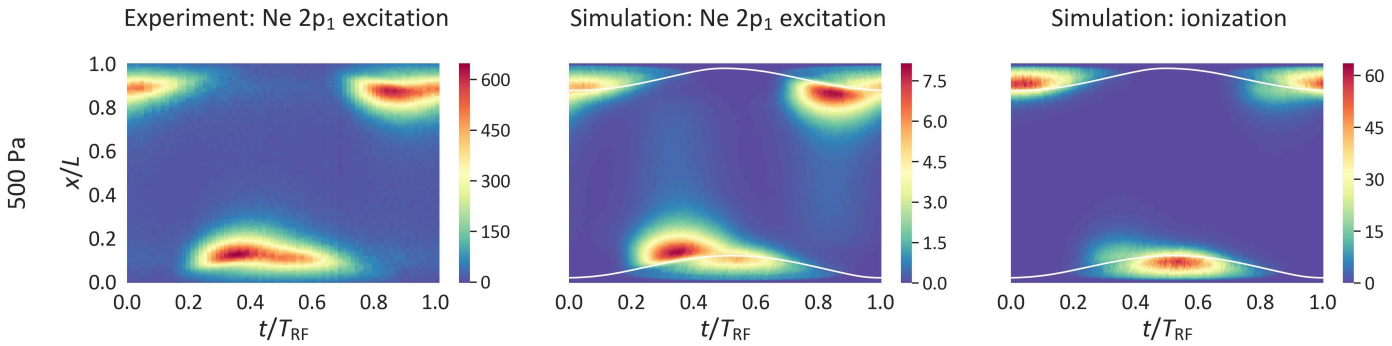

Figure *Spatio-temporal plots of the electron-impact excitation rate measured by PROES [a.u.] (left) and obtained from PIC/MCC [10^{19} $m^{-3}s^{-1}$] (center), and the ionization rate obtained from PIC/MCC [10^{20} $m^{-3}s^{-1}$] (right). The sheath edges are shown as white lines. The powered electrode is located at x/L = 0, while the grounded electrode is at x/L = 1. Discharge conditions: f = 6.78 MHz, L = 2.5 cm, V_{pp} = 330 V, p = 500 Pa. T_{RF} = 1/f.*

2019

Gas discharge physics. — Particle-in-Cell/Monte Carlo Collision (PIC/MCC) simulations have been performed to investigate the characteristics of geometrically symmetric capacitively coupled plasma sources in various gases and excited by different (single- and multi-harmonic) waveforms. In particular, we have investigated the effects of heavy-particle induced secondary electrons (SEs) on the ionization dynamics and on the control of ion properties (flux and energy distribution) at the electrodes [1], the dependence of the computed discharge characteristics on the assumptions on secondary electron emission coefficients of the electrodes [2] and on the electrode distance [3], as well as the electron kinetics and electron power absorption as a function of the mixing ratio of an electropositive (Ar) and an electronegative (CF_4) gas [4].

In our studies of the effect of heavy-particle induced secondary electrons [1] we have used radiofrequency excitation waveforms composed of up to four harmonics of the fundamental frequency of 13.56 MHz and "tailored" the driving voltage waveform by adjusting the identical phase angles of the even harmonics, θ. The simulations were carried out at neutral gas pressures of 3 Pa (nearly collisionless low-pressure regime) and 100 Pa (collisional high-pressure regime). Different approaches were used in the simulations to describe the secondary electron emission (SEE) at the electrodes: we adopted (i) constant ion-induced secondary electron emission coefficients (SEECs), γ, and (ii) realistic, energy-dependent SE yields for ions and fast neutrals. The mean ion energy at the electrodes was found to be controlled by θ at both pressures, for both approaches adopted to describe the SEE in the simulations. At a low pressure of 3 Pa, we obtained largely different dependencies of the ion flux at the electrodes on θ, depending on the value of the γ-coefficient. We have found that (i) at both pressures the surface conditions affect the plasma parameters and the quality of the separate control of ion properties at the electrodes and that (ii) adopting realistic, energy-dependent SE yields for heavy particles in the simulations can lead to significantly different results compared to those obtained by assuming constant SEECs. In [2], more details about the effect of γ on the electron power absorption dynamics, the plasma parameters and the quality of the separate control of ion flux and mean ion energy at the electrodes have been addressed. To demonstrate the effect of the choice of γ on modelling results, we carried out Particle-in-Cell/Monte Carlo Collision simulations of 13.56 MHz, single-frequency argon and helium capacitive discharges. The experimental investigations of the electrode distance on the plasma characteristics [3] were carried out in oxygen gas, at a fixed pressure of 2.66 Pa and a driving frequency of 13.56 MHz. We have found an increase of the central electron density with an increased electrode gap, while the time averaged optical emission of atomic oxygen lines decreased. These results were reproduced and understood by the PIC/MCC simulations performed under identical conditions. The simulations showed that the electron density increases due to a mode transition from the drift-ambipolar-mode (where the limited conductivity results in power absorption in the bulk part of the plasma) to the alpha-mode (where power absorption occurs near the edge of the expanding plasma sheath) induced by increasing the electrode gap. This mode transition was attributed to a drastic change of the electronegativity and the mean electron energy, which lead to the observed reduction of the emission intensity of an atomic oxygen line. More details about the electron power absorption mode transitions (the basic mechanism of energy coupling from an external power supply into the plasma) were uncovered using CF_4+Ar gas mixture plasmas [4] excited by tailored voltage waveforms in experimental investigations by phase-resolved optical emission spectroscopy, in conjunction with kinetic simulations and an analytical model. Single- and triple-frequency 'peaks'- and 'valleys'-type excitation waveforms (generated as a superposition of multiple consecutive harmonics of 13.56 MHz) were used at pressures of 20 and 60 Pa with 25 mm electrode gap and 150 V total driving voltage amplitude to determine the effects of the tailored driving voltage waveform in different gas mixtures. As the argon content in the buffer gas was increased the discharge switched from the drift-ambipolar power absorption mode to the alpha-mode (see Fig. 1). This transition was proven to occur due to the disappearance of the bulk and ambipolar electric fields as the electronegativity of the plasma decreased with increasing argon content.

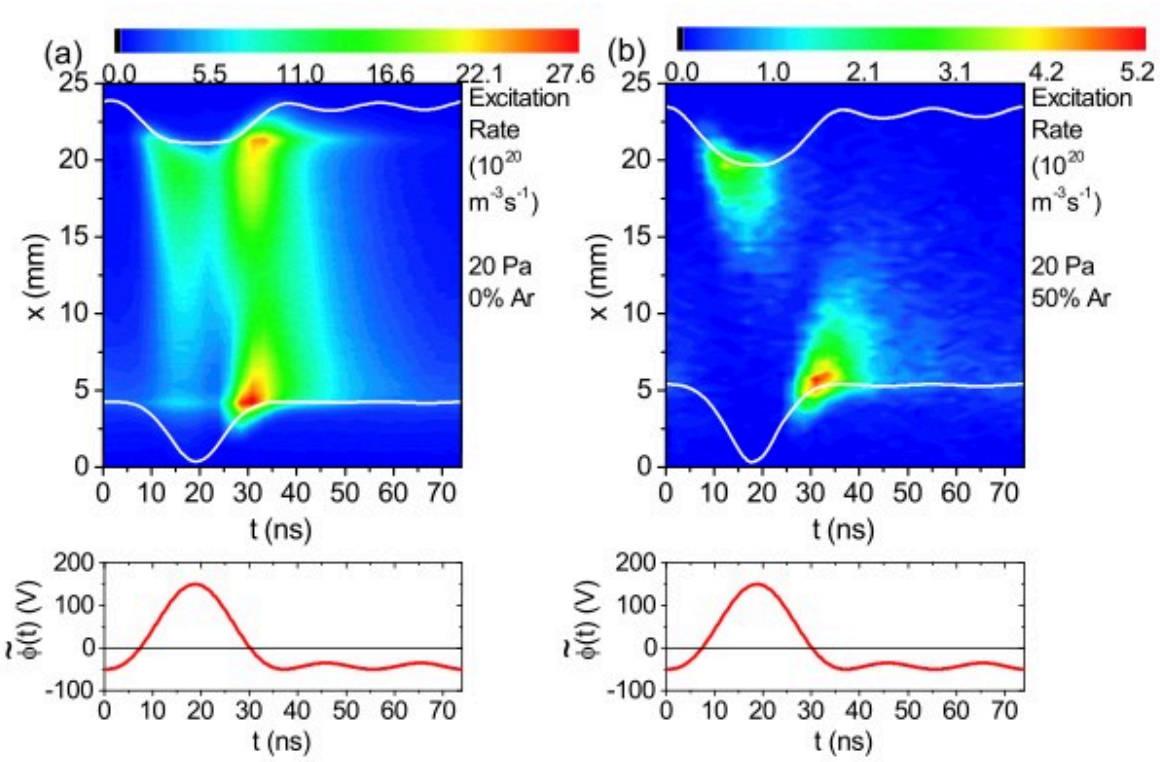

Figure 1. Spatio-temporal distribution of the electron impact excitation rate for the 703.7 nm fluorine line (excitation threshold energy: 14.56 eV) obtained from PIC/MCC simulations for the 'peaks'-waveform (3 harmonics, 150 V total voltage amplitude) at 20 Pa, in pure CF4 gas (a) and in 50% CF4 – 50% Ar mixture (b).

The sheath edges are marked by the white lines, the powered electrode is located at x=0 mm, while the grounded electrode is at x=25 mm. The panels in the second row illustrate the driving voltage waveform. Note the high excitation rate over the whole inner part of the plasma in (a) (characteristic for the drift-ambipolar mode) and the sharp maxima upon sheath expansion in (b) (characteristic for the alpha-mode) [4].

Complex plasmas. — The self-diffusion phenomenon in a two-dimensional dusty plasma at extremely strong (effective) magnetic fields was studied experimentally and by means of molecular dynamics simulations. In the experiment the high magnetic field was introduced by rotating the particle cloud and observing the particle trajectories in a corotating frame, which allows reaching effective magnetic fields up to 3000 T. The experimental results confirm the predictions of the simulations: (i) super-diffusive behavior is found at intermediate timescales and (ii) the dependence of the self-diffusion coefficient on the magnetic field is well reproduced [5].

In the many-body system of charged particles interacting via a pairwise Yukawa potential, the so-called Yukawa one-component plasma (YOCP), in the long-wavelength limit, the linear term in the dispersion of collective excitations defines the sound speed. The evolution of this from the weak-, through the strong-coupling regimes was investigated by analyzing the dynamic structure function S(k, ω) in the low-frequency domain. Depending on the values of Coulomb coupling and Yukawa screening five domains were identified in which the physical behavior of the YOCP exhibits different features. The competing physical processes are the collective Coulomb like versus binary-collision-dominated behavior and the individual particle motion versus quasilocalization. The theoretical results based on various models were compared in order to see which one provides the most cogent physical description and the best agreement with simulation data in the different domains [6].

A web-based platform was developed that allows users to perform molecular dynamics simulations, visualize the system for selected system parameters, and obtain results for the pair correlation function and the dispersion relation of waves in the system [7].

Reactive plasmas. – In the last decade plasma-activated water (PAW), or more generally plasma-activated liquid (PAL) has received a lot of attention from the plasma medicine and plasma agriculture community due to its potential to induce oxidative stress to cells. By PAL it is meant the liquid which contains reactive species, mostly reactive oxygen and nitrogen species (RONS), generated by the interaction of active or afterglow plasma with the liquid. PALs have been found to have antimicrobial and antibacterial effect, to have potentials for cancer therapy, and to improve the seeds germination and plant growth. The main long-lived RONS produced in PAL have been identified to be the H2O2, NO2– and NO3–. In order to be able to identify the role of different species and to clarify the synergy effects in the interaction of PAL with biological systems, PAL with different compositions would be welcomed, in what concerns the density ratios of different RONS. We have shown that a surface-wave microwave discharge is suitable to tune the ratio of active species concentrations over three orders of magnitude in deionized water (DIW), which can be preserved during months of storage at room temperature [8]. In order to control the ageing of PAWs, we have suggested the control of the H2O2 concentration by calling for a Fenton type of reaction with using copper surfaces.

External links:
[1] https://doi.org/10.1063/1.5100508
[2] https://doi.org/10.1088/1361-6595/ab094f
[3] https://doi.org/10.1063/1.5063543
[4] https://doi.org/10.1088/1361-6595/ab3c7c
[5] https://doi.org/10.1103/PhysRevE.99.013203
[6] https://doi.org/ 10.1103/PhysRevE.100.063206
[7] https://doi.org/10.1119/10.0000045
[8] https://doi.org/10.1088/1361-6595/ab3c2f

2018

We developed a particle-based simulation code for the description of short-pulsed (~ns) discharges at atmospheric pressure helium gas with an admixture of molecular nitrogen (at concentrations ≤1%). In this code, we have also included the photon treatment of the VUV resonance radiation of helium. We have explored the spatiotemporal evolution of charged species densities, reaction rates, and the fluxes of ”active” species at the surfaces. We have investigated, as well, the behaviour of the electron velocity distribution function and the electron energy probability function, and concluded that these deviate significantly from the Maxwell-Boltzmann distribution, especially in the cathode region of the discharge. These observations demonstrated the usefulness (and uniqueness) of particle simulations of similar physical systems. We have found that the VUV resonance radiation of He atoms is heavily trapped within the high-pressure gaseous environment and photons are

absorbed / re-emitted typically several hundred times before leaving the plasma. Nonetheless, the escaping photons were found to contribute significantly to the electron emission process at the electrodes. For most conditions studied, an increase of around a factor of two of the current pulse peak was observed when VUV photons were included in the simulations, in comparison to those cases when their effect was neglected. The figure shows results for a plane-parallel electrode configuration with a gap of 1 mm, to which a high voltage pulse with an amplitude of 1000 V is applied, with a trapezoidal shape. Current pulses in the order of 10 A are generated over the electrode surface of 1 cm^2, when VUV photons are not considered in the simulation (at an initial charged particle density of 1.5×10^{11} cm^{-3}). The peak current grows to ~20 A, when VUV photons are included. The figure also shows the time integrated wavelength-resolved radiation from the plasma, in the vicinity of the theoretical wavelength of the $2^1P \rightarrow 1^1S$ resonant transition.

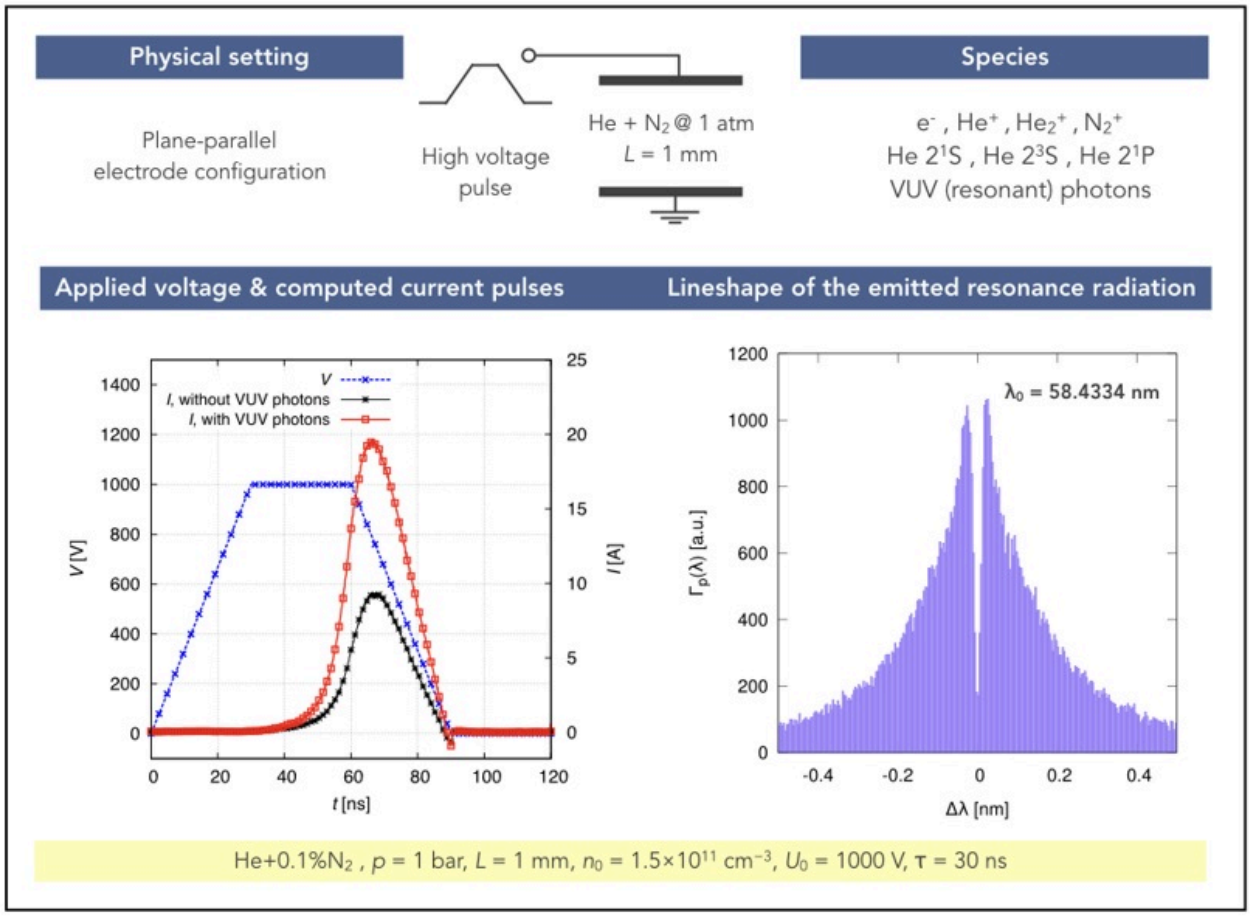

We have performed systematic investigation of the influence of various surface processes - such as the secondary electron (SE) emission induced by ions and electrons, and electron reflection at the electrodes - on the discharge characteristics in low-pressure capacitively coupled radiofrequency discharges. By using a realistic (energy-dependent) model for the description of the electron-surface interaction in our Particle-in-Cell/Monte-Carlo Collisions (PIC/MCC) simulation code, we have studied the effect of the electron-induced SEs on the discharge characteristics in the 0.5 Pa–3 Pa pressure range, for voltage amplitudes between 100 V–1500 V, assuming different SE yields for ions (γ–coefficient). Such discharge conditions are typical in industrial applications, such as plasma etching, sputtering and plasma immersion ion implantation. We demonstrated that the realistic description of the electron-surface interaction significantly alters the computed plasma parameters, compared to results obtained based on a simple model (which completely neglects the emission of SEs due to electron impact) for the description of the electron-surface interaction, widely used in PIC/MCC simulations of low-pressure capacitively coupled plasmas.

We have found that both the gas pressure and the value of the γ-coefficient affect the role of electron induced SEs (δ-electrons) in shaping the discharge characteristics at different voltage amplitudes. Their effect on the ionization dynamics has been found to be most striking at low pressures, high voltage amplitudes and high values of the γ-coefficient (see Figure 1). At low pressures, the energetic ion-induced SEs (γ -electrons) generated at one electrode and accelerated towards the bulk by the local sheath electric field, can cross the bulk without collisions and generate a high number of electron-induced SEs (δ-electrons) upon their impact at the opposite electrode. Depending on the instantaneous local sheath voltage, these δ-electrons are accelerated into the plasma bulk, where they generate significant ionization and enhancement of the plasma density. On the other hand, at high pressures due to the more frequent collisions, the electrons reach the electrodes at lower energies, which leads to a decrease of the number of SEs emitted by electron impact at the electrodes, therefore, to a decrease of the contribution of δ-electrons to the ionization.

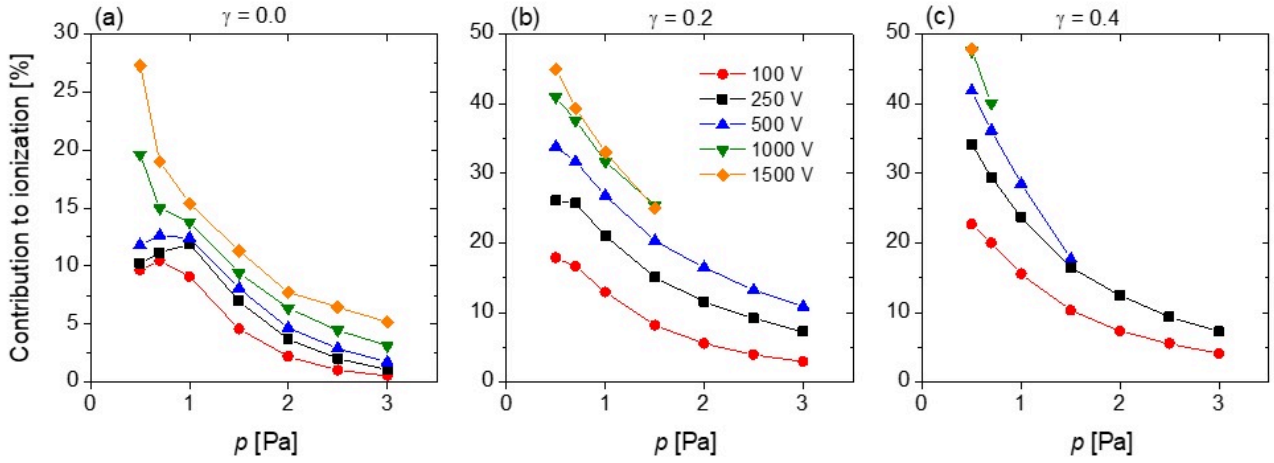

Figure 1. *Contribution of electron-induced secondary electrons (δ-electrons) to the total ionization at different pressures and voltage amplitudes, for different values of the ion-induced secondary electron emission coefficent, γ.*

Dusty plasmas –
In the field of dusty plasma physics we have realized a rotating electrode experiment to measure the diffusion of highly charged dust particles in large external quasi-magnetic field. We have shown that with increasing magnetization the transport becomes hindered and the non-Maxwellian nature becomes more prominent as strong super-diffusion is observed. Our experimental results are supported by molecular dynamics simulations of magnetized Yukawa systems. In relation to the PK-4 dusty plasma experiment onboard the International Space Station (ISS) we have implemented a cylindrical 2D particle-in-cell with Monte Carlo collisions (PIC/MCC) numerical simulation for direct current neon discharged. Our results indicate, that the apparent quiet positive column as observed in the experiment with long exposure time imaging is in fact made of quickly moving ionization waves, as shown in Figure 2. Our numerical prediction has been confirmed by fast camera imaging experiments. The presence of ionization waves explains the unexpected observation of dominant dust particle chain formation in the micro-gravity setup.

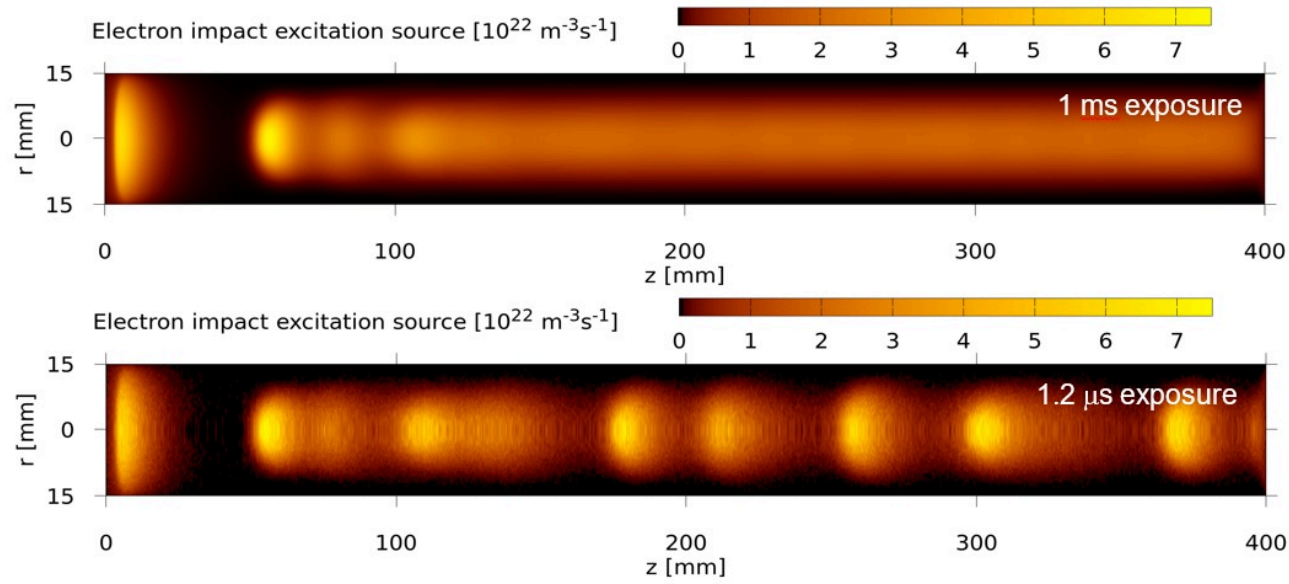

Figure 2. *Electron impact excitation source from the PK-4 neon discharge simulation at long and short exposure times.*

Reactive plasmas –
In the last decade plasma-activated water (PAW), or more generally plasma-activated liquid (PAL) has received a lot of attention from the plasma medicine and plasma agriculture community due to its potential to induce oxidative stress to cells. By PAL it is meant the liquid which contains reactive species, mostly reactive oxygen and nitrogen species (RONS), generated by the interaction of active or afterglow plasma with the liquid. PAW has been found to have antimicrobial and antibacterial effect, which is thought to occur due to the synergetic effect between the RONS and/or pH of the solution. Plasma activated buffered solution and cell culture media has also been studied for therapeutical aims, and it has been shown its potentials for cancer therapy. In the field of

agriculture with PAW the improvement of seeds germination and plant growth have been targeted. The main long-lived RONS produced in PAL have been identified to be the H_2O_2 , NO_2– and NO_3–. The usual studies report typically one or two PAL conditions, giving no further suggestions for PAL composition tuning. In order to be able to identify the role of different species and to clarify the synergy effects in the interaction of PAL with biological systems, PAL with different compositions would be welcomed, in what concerns the density ratios of different RONS.

With our study we have shown the possibility of tunning the ratio of active species concentrations over three orders of magnitude in deionized water (DIW) activated with a surface-wave microwave discharge, see Figure 3, by varying the gas flow rate, initial gas mixture composition and treatment distance. The surface-wave microwave discharge is generated with the help of a surfatron launcher in a quartz tube of outer diameter 6 mm and inner diameter 4 mm using as a main gas Ar at gas flow rates of 1500 and 2000 sccm (Ar_x conditions in Figure 3). Ar-N_2/O_2 binary (ArN_2_x and ArO_2_x conditions) and ternary (ArN_2O_2_x conditions) mixtures are also used with the O_2 and N_2 gas flow rates ranging between 10-100 sccm. The input power is varied between 25 and 30 W, and the DIW is positioned below the plasma plume with the water surface being at d = 5.5 - 10.5 mm distance from the edge of the quartz tube, see Figure 4. By changing the mixture composition and the treatment distance, at the plume - water surface interaction point the electron density is changed, which determines the concentration of H_2O_2 created in the liquid phase.

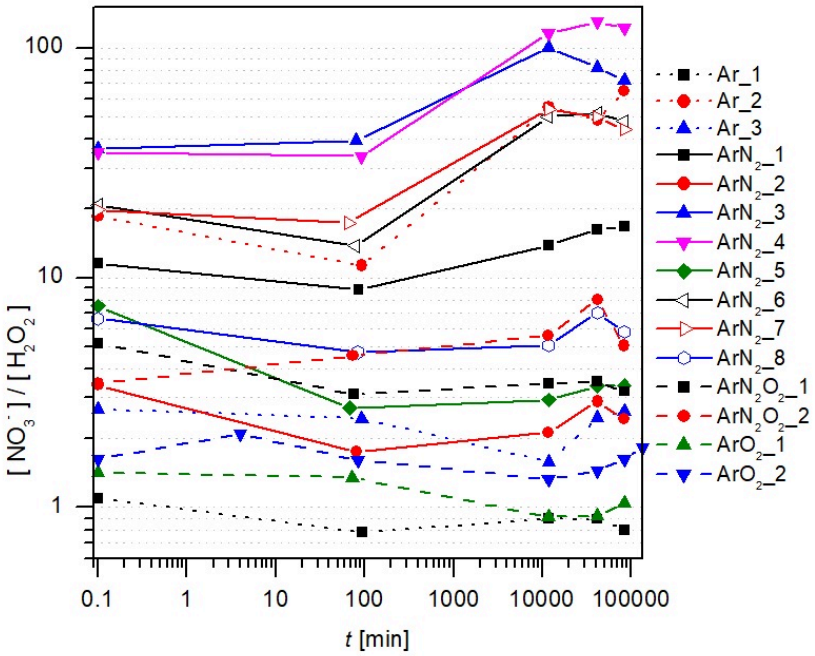

Figure 3. *The ageing of the nitrate to hydrogen peroxide concentration ratio in the case of PAWs produced by Ar/N2/O2 surface-wave microwave discharges at different discharge and treatment conditions.*

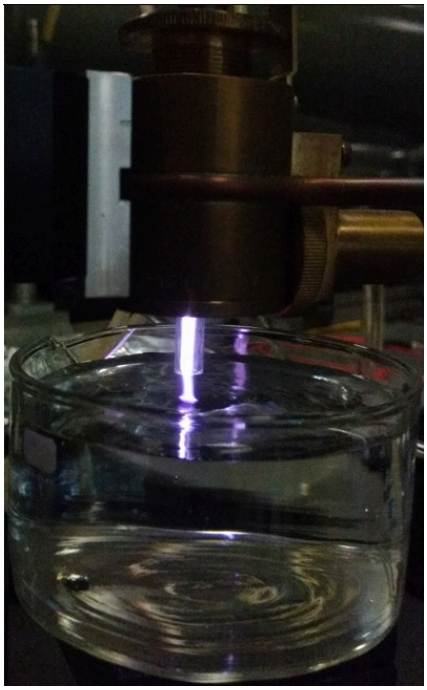

Figure 4. *A surface-wave microwave discharge in interaction with water surface.*

2017

Gas discharge physics. – We have addressed several aspects of charged particle kinetics and transport in low-temperature plasmas. Particular attention has been devoted to the non-linear effects, like the spontaneous pattern formation in electronegative discharge plasmas driven by radiofrequency (RF) voltage sources. In strongly electronegative gases, like carbon-tetraflouride, a positive ion – negative ion plasma is formed with a strongly depleted electron density, due to the (dissociative) electron attachment to molecules, which this way form negative ions. We have shown that a resonance between the excitation (radio) frequency and the eigenfrequency of the ion-ion plasma leads to an instability, which, in turn, creates prominent non-linear structures. The dependence of this pattern formation mechanism on the discharge conditions, such as the driving voltage amplitude and frequency, as well as the electrode separation and gas pressure, has been studied in detail.

By using our Particle-in-Cell/Monte-Carlo Collisions (PIC/MCC) simulation code, we have investigated the electron heating and ionization dynamics in capacitively coupled oxygen discharges driven by tailored voltage waveforms at different fundamental frequencies and at different pressures. We have found transitions of the discharge electron heating mode from the drift-ambipolar mode to the α-mode, induced by changing the number of consecutive harmonics included in the driving voltage waveform or by changing the gas pressure. We have found that changing the number of harmonics in the waveform has a strong effect on the electronegativity of the discharge, on the generation of the DC self-bias and on the control of ion properties at the electrodes. Furthermore, we have investigated the effect of the surface quenching rate of O2(a) metastable molecules on the spatio-temporal excitation patterns. We have obtained good agreement between the spatio-temporal distributions of the excitation rates obtained from the simulations and those derived from phase-resolved optical emission spectroscopy measurements. This benchmarking study was complemented with a sensitivity analysis of the results on the rates of selected plasma-chemical reaction processes.

We have developed a realistic model for the description of the electron-surface interaction in capacitively coupled plasmas and incorporated this model into our PIC/MCC simulation code. This realistic model considers the elastic reflection and the inelastic backscattering of electrons, as well as the emission of electron-induced secondary electrons taking into account the properties of the surface. By using this model, we have studied the influence of the electron-induced secondary electrons on the plasma parameters in argon gas at low pressures, for SiO2 electrodes. Compared to the results obtained by using a simplified model for the electron-surface interaction, we have found that the electron-surface interactions strongly influence the electron power absorption and ionization dynamics (see Fig. 1).

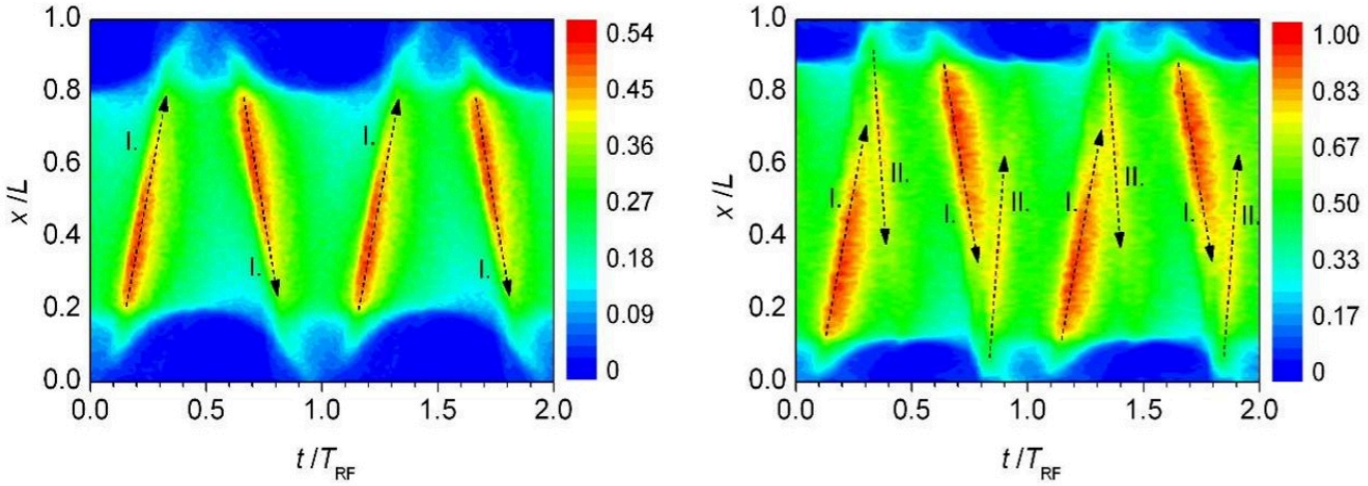

Figure 1. *PIC/MCC simulation results on the spatio-temporal distributions of the ionization rate [1021m-3s-1], based on a simplified model (left plot) and a realistic model (right plot) for the electron-surface interaction.*

Discharge conditions: argon, SiO2 electrodes, 6.7 cm electrode gap, 0.5 Pa, 13.56 MHz, 1000 V. The horizontal axis corresponds to two RF periods. The vertical axis shows the normalized distance from the powered to the grounded electrode.

Strongly coupled plasmas. – In the field of strongly coupled plasmas (SCP), we have contributed by molecular dynamics simulations to the validation of the theoretical "method of moments" approach, which allows the determination of the characteristics of the collective modes (including their damping), based solely on static characteristics (i.e., the static structure factor, or the pair correlation function) of the plasma. We presented the first experimental measurement of the 3-point static structure factor, S(3)(k1,k2,k0), of a 2-dimensional dusty plasma liquid. The higher-order structure factor was as well computed from molecular dynamics simulations and very good agreement was obtained between the two sets of data (see Fig. 2). Both the measurements and the simulations confirmed the existence of negative values of S(3)(k1,k2,k0); this indicates the breakdown of the convolution approximation that gives S(3)(k1,k2,k0) in a factorized form of S(2)(2-point) functions. According to the quadratic fluctuation-dissipation theorem, a changing sign of S(3)(k1,k2,k0) implies a sign change of the quadratic part of the density response function of the system and an intriguing vanishing quadratic response at a certain wavenumber.

Dusty plasmas. – In the field of dusty plasma physics, we have developed a new, very simple and sensitive method to measure the sputtering rate of solid materials in stationary low-pressure gas discharges. The method is based on the balance of the centrifugal force and the confinement electric force acting on a single electrically charged dust particle in a rotating environment. We have demonstrated the use and sensitivity of this method in a capacitively coupled radio frequency argon discharge. We were able to detect a reduction of 10 nm in the diameter of a single dust particle and have measured the reduction rate of 6 nm/min of the particle radius.

A magnetic field was recently shown to enhance the field-parallel heat conduction in a strongly correlated plasma whereas cross-field conduction is reduced. With three-dimensional molecular dynamics simulations relevant to dusty plasmas, we have shown that in such plasmas, the magnetic field has the additional effect of inhibiting the isotropization process between field-parallel and cross-field temperature components, thus leading to the emergence of strong and long-lived temperature anisotropies when the plasma is locally perturbed. We have presented an extended heat equation, which is able to describe this process accurately.

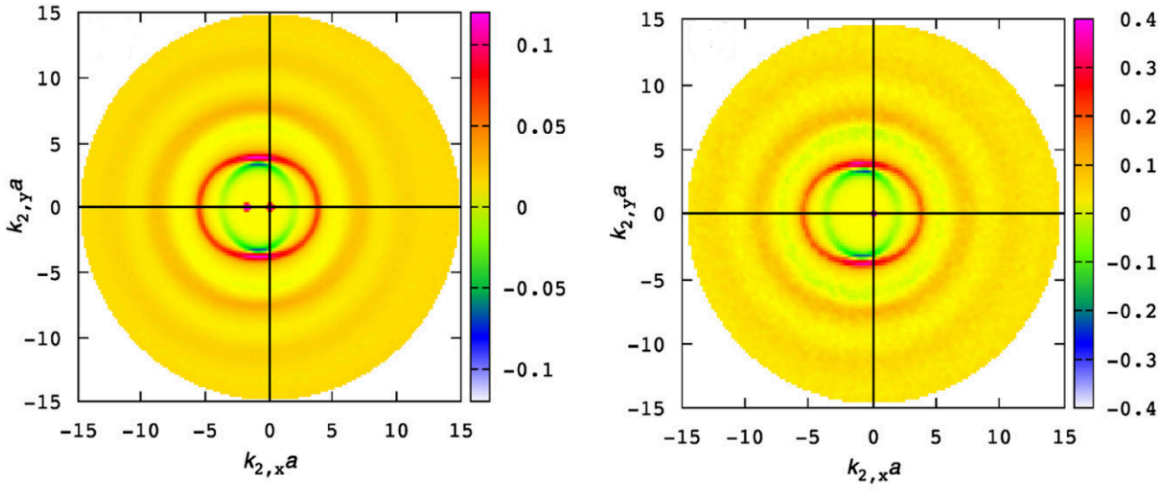

Figure 2. *Maps of the full* S(3)(k1,k2,k0) *3-point static structure factor of strongly coupled Yukawa-liquids at a wave vector k1a = (1.85,0). Left: experimental data obtained on a 2-dimensional dusty plasma, right: results of molecular dynamics simulations at the same plasma parameters (a coupling coefficient of 95 and a screening coefficient of 0.7).*

Technological application of high-frequency discharge systems. – Based on our experience gained during the biological decontamination studies on afterglow plasmas, we have joined another fast-developing field, namely plasma agriculture, which is aimed to develop new technology for agriculture. We used the afterglow of a surface-wave microwave discharge to investigate the effect of different afterglow plasmas on cereal crops. In our study, we treated non-infected and infected cereal crops, respectively, in the afterglow of Ar/N2-O2 surface-wave microwave discharges at 2-8 mbar pressure, using the following initial gas mixtures: (i) N2-20%O2, (ii) N2-10%O2, (iii) N2-2%O2, (iv) Ar-20%O2, (v) Ar-40%O2 and (vi) Ar-20%O2 + N2-2%O2, which made possible to isolate different species and identify their role in the process. We have shown that the germination and vigour of non-infected seeds are not significantly effected when barley is treated max 120 s at 2 mbar and maize 240 s at 4 mbar. On the other hand, seeds can be disinfected from the germination inhibitors F. graminearum and F.

verticillioides. The most efficient treatment, which also increases the germination of infected seeds above 80%, is the 3 min Ar-20%O2 afterglow at 4 mbar for barley, while for maize the 4 min Ar-20%O2+2 min N2-2%O2 afterglow at 8 mbar. The high NO-content mixtures and the heating of seed surface by the recombination of O and N-atoms inhibit barley germination.

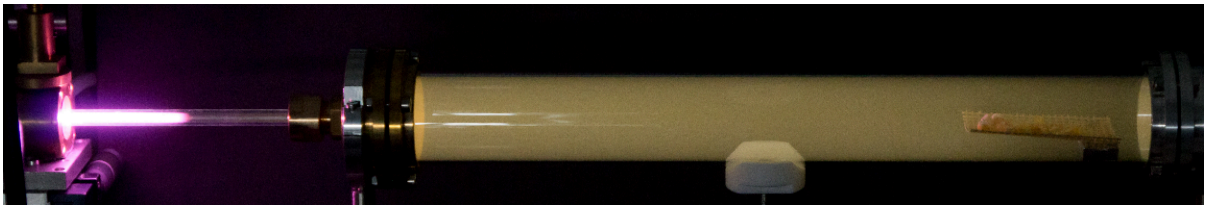

Figure 3. *The post-discharge system with the surface-wave microwave discharge operating in N2-20%O2 mixture during seed treatments.*

We have studied the formation of oxide structures on copper plates in the discharge sheath and in the afterglow region of an inductively coupled rf discharge at different gas mixtures, input power and treatment time, as well as in the afterglow of a surface-wave microwave (mw) discharge, and compared the two systems. In the sheath of the rf discharge, regular shapes have been formed with incipient growth of nanowires as shown in Fig. 4 (a). Higher power, which results in higher temperature, contributed to thicker layer formation, while lower powers to the structuring of the oxide layer. The oxidation in the afterglow was found to be much faster, in few minutes a thick layer was formed which detached after a threshold thickness. Depending on the oxygen content and gas temperature, different structures could be created. At lower O2 content mixture (50 sccmAr-10 sccm O2), larger individual structures have been formed, with the attempt of wires to grow on them. At the same low flow rate, with further decrease of the input power, wall structures were found, and, similarly, also in the afterglow of the mw discharge at 500 sccm N2 – 120 sccm O2. Fig. 4 (b)-(c) show the restructuring of the copper-oxide layer created in RF afterglow with the N2-O2 mw afterglow, showing the wall shape structuring of the initial structures. In case of Ar-O2 mw discharge, the oxidation rate is very low due to the lower temperature compared to the N2-O2. We have found that the wall structure, which is the basic element of the structures, can be created at lower oxidation rate, which is related to lower temperature and lower O-atom density. In case of a surface-wave microwave discharge system, this can be easily tuned with the gas flow rate and the position of the wave launcher along the discharge tube.

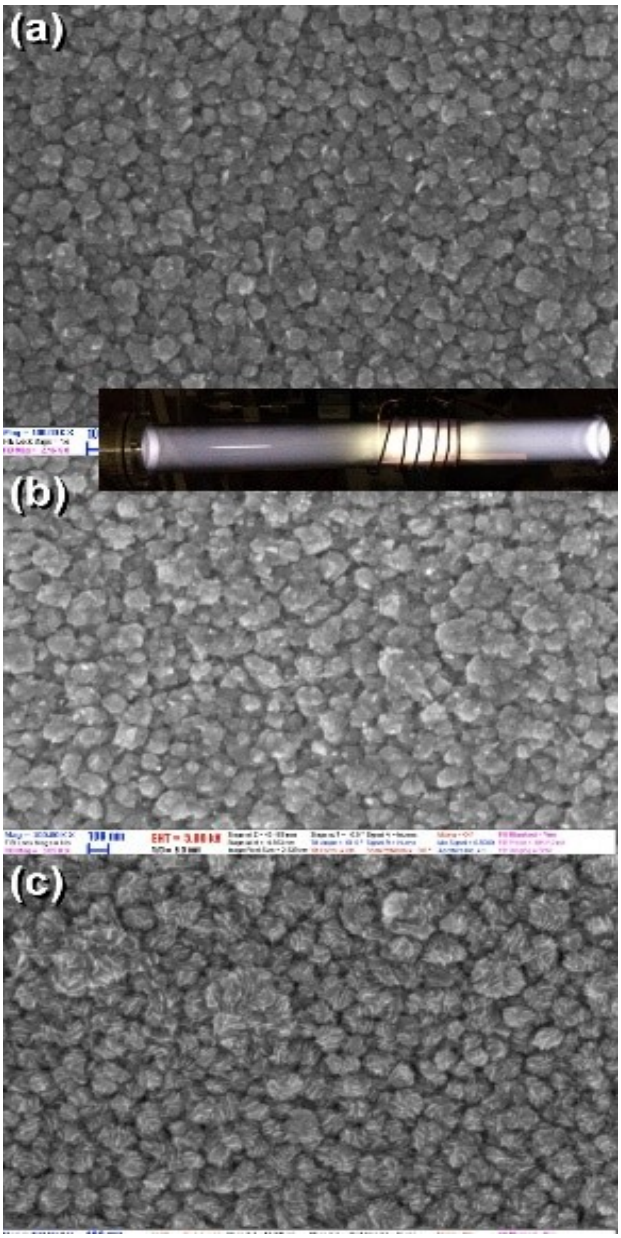

Figure 4. *(a) Copper-oxide surfaces created in the discharge region of the 50 sccm O2, 50 W rf discharge. (b) The copper-oxide surface created in the afterglow of the 10 sccm O2, 20 W rf discharge. (c) The (b) surface restructured in the N2-O2 mw afterglow.*